

Doctoral Thesis

Critical conditions of degradation during  
thermochemical hydrogen compression by  
 $V_{20}Ti_{32}Cr_{48}$  alloy

GUO FANGQIN

Graduate School of Integrated Arts and Sciences  
Hiroshima University

September 2020



Doctoral Thesis

Critical conditions of degradation during  
thermochemical hydrogen compression by  
 $V_{20}Ti_{32}Cr_{48}$  alloy

GUO FANGQIN

Division of Integrated Arts and Sciences  
Graduate School of Integrated Arts and Sciences  
Hiroshima University

September 2020



## 1. Thesis Title

Critical conditions of degradation during thermochemical hydrogen compression by  $V_{20}Ti_{32}Cr_{48}$  alloy

## 2. Research Article

Critical temperature and pressure conditions of degradation during thermochemical hydrogen compression: A case study of V-based hydrogen storage alloy

## 3. Co-authored Article

1. Deliquescence behavior of photo-irradiated single  $NaNO_3$  droplets
2. In Situ Observation of Efflorescence and Deliquescence Phase Transitions of Single  $NaCl$  and  $NaNO_3$  Mixture Particles in Air Using a Laser Trapping Technique
3. Iron based catalyst for the improvement of the sorption properties of  $KSiH_3$



# Abstract

Hydrogen as a clean energy attracted a lot of attentions and becoming a promising technology to help us to build a sustainable and renewable society in the future. The development of excellent hydrogen storage materials and the evaluation of their hydrogen storage behaviors are very important steps for establishing basic infrastructure and hydrogen industrial chain. Disproportionation and phase separation of hydrogen storage materials are big issues that occurred under extreme pressure and temperature conditions during prolonged hydrogen compressor cycles, which make metal hydrides inactive and reduce their compression efficiency. Thus, it is important to identify boundary conditions to avoid such unwanted phase separation. However, no investigation related to this problem has been carried out by practical experiment so far. Thus, in this thesis, systematic investigations were conducted to find the critical conditions of hydrogen compressor cycle test for  $V_{20}Ti_{32}Cr_{48}$  alloy as a model system for the first time.

The initial hydrogen amount was precisely fixed according to pressure composition isotherm(PCI) measurements of  $V_{20}Ti_{32}Cr_{48}$  alloy: four different points were selected as starting points according to different hydrogen content on desorption curve, namely, solid solution (0%  $\beta$ -phase), half saturated (50%  $\beta$ -phase), 75% saturated (75%  $\beta$ -phase), and fully saturated (100%  $\beta$ -phase). Hydrogen compressor cycle tests were conducted for 25 cycles with same amount of  $V_{20}Ti_{32}Cr_{48}$  alloy with various hydrogen content and temperature conditions individually. Main finding and results are summarized as follows:

First of all, the influence of hydrogen content on the cyclic durability of  $V_{20}Ti_{32}Cr_{48}$  alloy was given the priority to be studied. It was found that after 25 hydrogen compressor cycles up to higher temperature (100% saturated up to 240 °C, others up to 260 °C), the

hydrogen storage properties of  $V_{20}Ti_{32}Cr_{48}$  alloy with fully and 75% saturated  $H_2$  were deteriorated a lot and 20.2% and 22.7% reduction in hydrogen storage capacity was observed respectively with sloppy plateau region. The increased slope indicated the possibility of multiple phases present in the sample, which dramatically reduced hydrogen compression efficiency. On the other hand,  $V_{20}Ti_{32}Cr_{48}$  alloy with 50% saturated  $H_2$  and solid solution, the hydrogen storage capacity losses were found to be negligible, 5.0 and 4.0% respectively, with similar slope in PCI curves, indicating the intact hydrogen compression efficiency during cycling. Structure and morphology changes measured by XRD and SEM provided the direct evidence that the disproportionation and phase separation occurred in the sample of  $V_{20}Ti_{32}Cr_{48}$  alloy with fully saturated  $H_2$  from the appearance of multiple and overlapped peaks in forms of  $VH_{0.88}$  and  $TiH_{0.66}$ . In addition, the sample with initial 75% saturated  $H_2$  for hydrogen compressor at 260 °C undergone through a reduction in capacity, however no big changes in peaks position was observed except the alteration in peak width and intensity which might be caused by stress/strains. Thus it is concluded that the phase separation is not the only reason for capacity fading, but the stress/strain generated in the material during the compressor test may also be responsible for this degradation. Based on the above results, lower hydrogen content was found to be better for hydrogen compressor cyclic durability of  $V_{20}Ti_{32}Cr_{48}$  alloy whereas the large amount of stored hydrogen in alloy led to the reduction of reversible hydrogen storage capacity during hydrogen compression process for practical usage. This resulted in lowering compression efficiency and the increase in the maintenance cost.

Besides the hydrogen content influence on the cyclic durability of  $V_{20}Ti_{32}Cr_{48}$  alloy, temperature impact should also not be negligible. Thus, temperature influence on the cyclic durability for  $V_{20}Ti_{32}Cr_{48}$  alloy employed for compressor was also investigated for

the maximum temperature as 240, 200, 175, 150, and 100 °C individually. The PCI curves of  $V_{20}Ti_{32}Cr_{48}$  alloy, fully saturated with  $H_2$  and cycled for hydrogen compressor up to 240 °C and 200 °C showed significant hydrogen storage capacity loss up to 20.2% and 17.9% respectively, revealing the disproportion and degradation of the materials. On the other hand, the same alloy cycled up to 175, 150 and 100 °C showed little hydrogen capacity losses around 4 to 5% with similar PCI slope and stable hydrogen storage capacity. The appearance of the new phases,  $VH_{0.88}$  and  $TiH_{0.66}$  in XRD pattern, and the Ti-rich phase found by SEM-EDS results clearly showed the disproportionation of  $V_{20}Ti_{32}Cr_{48}$  alloy with fully saturated  $H_2$ , which is caused by thermodynamically favored reactions. In addition, 200 °C may not be high enough to lead such kind of reaction but could generate lattice stress / strains in the alloy which causes the reduction in hydrogen storage capacity after compressor cycling test. Thus lower temperature was found better for the compressor cyclic durability of  $V_{20}Ti_{32}Cr_{48}$  alloy. Whereas, higher temperature resulted in the degradation of this alloy and reduced the hydrogen storage capacity during practical usage.

In summary, hydrogen content as well as temperature both play an important role in the disproportionation processes. The threshold about hydrogen content and temperature of  $V_{20}Ti_{32}Cr_{48}$  alloy for hydrogen compressor without disproportionation were identified as 75% and 200 °C respectively. Operation conditions should not be beyond these threshold values if we want to use  $V_{20}Ti_{32}Cr_{48}$  alloy for hydrogen compressor safely and efficiently. This methodology can be employed to be used with other materials to identify the critical conditions required for their safer and stable operation during hydrogen compressor cycling.

# Acknowledgements

I would like express my acknowledgement to all the people who had helped and supported me during the past 3 years of my Ph.D. study together with one year's baby caring. Thanks to them, I have enough courage and confidence to finish my study and become a good mother at the same times at Hiroshima University, where my experimental skills and knowledge about hydrogen storage field as well as logical and scientific thinking have been developed a lot.

First of all, I would like to express my great appreciation to my supervisor, Professor Takayuki Ichikawa for his patient guidance, enthusiastic encouragement and useful suggestions during my whole PhD study life. He is such a nice, gentle, energetic and knowledgeable researcher who can always have a lot of innovative and unique ideas for the guidance of my study. He gave me a lot of support in my daily life and I am very grateful for his effort on helping me applying many scholarships.

Second, I would like to offer my special thanks to Associate Professor Ankur Jain for teaching me how to operate experimental equipment and how to finish experiments efficiently and safely. He always gave me many instructive advices on my research which helped me a lot. He is also a warmhearted person who actively encouraged me when I was upset.

Then, I am particularly grateful to Professor Yoshitsugu Kojima, and Associate Professor Hiroki Miyaoka for their useful suggestion and discussion for my research.

I wish to acknowledge the help provided by my senior Dr. Suganthamalar Selvaraj for her kind help in PCT measurements and the help from Mr. Tomoyuki Ichikawa for his supporting in making sample cell and solving various technical problems.

Assistance provided by Mr. Keita Shinzato and Ms. Pratibha Pal is greatly appreciated for helping me to finish several experiments.

I wish to acknowledge all the help provided by our secretary Ms. Misao Mukouda and Ms. Saori Inagaki for their kind support of my daily life. I would like to thank all the members in our lab for their assistance.

In the end, my special thanks will be given to my family member, my husband Dr. Yufeng Wang, who has accompanied me from undergraduate study. He always supported me and gave me a lot of advices. Thanks to the coming of our dear daughter Qingzhu Wang, I became a strong mother and was able to overcome every difficulty in my PhD life. I am very grateful for the support and understanding of our parents, my sister, and all the relatives, who helped me a lot to have a new life in Japan.

## Contents

<b>1.</b>	<b>Introduction</b> .....	<b>1</b>
1.1	Hydrogen energy.....	1
1.2	Hydrogen storage methods .....	2
1.2.1	Storage in compressed state .....	3
1.2.2	Storage in liquid state .....	5
1.2.3	Storage in solid state .....	6
1.3	Hydrogen absorption/desorption properties of hydrogen storage materials .....	8
1.3.1	Hydrogen absorption/desorption characteristics of hydrogen storage materials .....	8
1.3.2	Thermodynamics of hydrogen storage.....	11
1.4	Hydrogen storage alloys developed for hydrogen compression	13
1.4.1	AB <sub>5</sub> type alloys.....	13
1.4.2	AB <sub>2</sub> type alloys.....	15
1.4.3	AB type alloys .....	17
1.4.4	BCC type alloys .....	18
1.5	Recent development of hydrogen compressor .....	19
	<b>Figures</b> .....	<b>23</b>
<b>2.</b>	<b>Purpose of this thesis</b> .....	<b>26</b>
<b>3.</b>	<b>Experimental</b> .....	<b>29</b>
3.1	Sample preparation .....	29
3.2	Activation process.....	29

<b>3.3</b>	<b>X-ray diffraction (XRD)</b> .....	30
(1)	<b>Basic principle</b> .....	30
(2)	<b>Measurement procedure</b> .....	31
<b>3.4</b>	<b>Scanning electron microscopy (SEM)</b> .....	31
(1)	<b>Basic principle</b> .....	31
(2)	<b>Measurement procedure</b> .....	33
<b>3.5</b>	<b>Energy dispersive X-ray spectroscopy (EDS)</b> .....	33
(1)	<b>Basic principle</b> .....	33
(2)	<b>Measurement procedure</b> .....	34
<b>3.6</b>	<b>Pressure composition isotherm measurement (PCI)</b> .....	34
(1)	<b>Basic principle</b> .....	34
(2)	<b>Measurement procedure</b> .....	37
<b>3.7</b>	<b>Hydrogen compressor cycle system</b> .....	37
<b>Figures</b>	.....	39
<b>4.</b>	<b>Results and discussions</b> .....	45
<b>4.1</b>	<b>Hydrogen storage properties of <math>V_{20}Ti_{32}Cr_{48}</math> at room temperature</b> .....	45
<b>4.2</b>	<b>The influence of hydrogen content on the cyclic durability of</b> <b><math>V_{20}Ti_{32}Cr_{48}</math> alloy</b> .....	46
<b>4.2.1</b>	<b><math>V_{20}Ti_{32}Cr_{48}</math> alloy hydrogen storage behavior comparison by</b> <b>PCI</b> .....	46
<b>4.2.2</b>	<b>hydrogen compressor cycling test of <math>V_{20}Ti_{32}Cr_{48}</math> alloy</b> .....	48
<b>4.2.3</b>	<b>Structure and phase characterization of <math>V_{20}Ti_{32}Cr_{48}</math> alloy by</b>	

<b>X-ray diffraction.....</b>	<b>49</b>
<b>4.3 Temperature influence on the cyclic durability of V<sub>20</sub>Ti<sub>32</sub>Cr<sub>48</sub> alloy .....</b>	<b>50</b>
<b>4.3.1 Hydrogen compressor cycling test of V<sub>20</sub>Ti<sub>32</sub>Cr<sub>48</sub> alloy with fully saturated H<sub>2</sub> up to different temperatures .....</b>	<b>51</b>
<b>4.3.2 Temperature influence on the cyclic durability of V<sub>20</sub>Ti<sub>32</sub>Cr<sub>48</sub> alloy with fully saturated H<sub>2</sub> content.....</b>	<b>52</b>
<b>4.3.3 Temperature influence on the cyclic durability of V<sub>20</sub>Ti<sub>32</sub>Cr<sub>48</sub> alloy with half saturated H<sub>2</sub> content.....</b>	<b>53</b>
<b>4.3.4 Temperature influence on the cyclic durability of V<sub>20</sub>Ti<sub>32</sub>Cr<sub>48</sub> alloy with solid solution of hydrogen.....</b>	<b>54</b>
<b>4.3.5 Structure and phase characterization of V<sub>20</sub>Ti<sub>32</sub>Cr<sub>48</sub> alloy with different hydrogen content under temperature influence by X-ray diffraction.....</b>	<b>55</b>
<b>4.4 Structural and morphology investigation of pristine and disproportionated V<sub>20</sub>Ti<sub>32</sub>Cr<sub>48</sub> alloys by SEM and EDS mapping technique .....</b>	<b>56</b>
<b>4.5 Summary of hydrogen compressor test of V<sub>20</sub>Ti<sub>32</sub>Cr<sub>48</sub> alloy.....</b>	<b>58</b>
<b>Figures .....</b>	<b>62</b>
<b>Tables .....</b>	<b>82</b>
<b>5. Conclusions .....</b>	<b>84</b>
<b>References: .....</b>	<b>88</b>

## List of Figures

<b>Figure 1.1</b> Primitive phase diagram of hydrogen under different temperature and pressure conditions .....	23
<b>Figure 1.2</b> Pressure-composition-isothermal (PCI) measurements and a Van't Hoff curve (logarithm of the plateau pressure against the reciprocal temperature); values are for LaNi <sub>5</sub> . .....	24
<b>Figure 1.3</b> Illustration of the procedure of hydrogen gas reacting with metal alloys .....	25
<b>Figure 3.1</b> Schematic representation of the diffraction of X-rays from crystal planes .....	39
<b>Figure 3.2</b> (a) Rigaku-RINT 2500 X-ray diffraction equipment used in this work, (b) sample plate for XRD. ....	40
<b>Figure 3.3</b> (a) Interaction between the incident electron beams with the material, (b) sample plate for SEM-EDS.....	41
<b>Figure 3.4</b> Diagram of generation of characteristic X-ray .....	42
<b>Figure 3.5</b> (a) The PCI measurement system used in this study; (b) the schematic illustration of the PCT measurement system. ....	43
<b>Figure 3.6</b> Homemade hydrogen compressor cycling test system.....	44
<b>Figure 4.1</b> PCI curve of V <sub>20</sub> Ti <sub>32</sub> Cr <sub>48</sub> alloy at room temperature. ....	62

**Figure 4.2** Room temperature PCI curves of  $V_{20}Ti_{32}Cr_{48}$  alloy (a) before and after (b-e) 25 hydrogen compressor cycling tests up to high temperature (b: up to 240°C and c, d and e: up to 260°C). The starting point was decided according to different hydrogen content: a) solid solution, b) half saturated, c) 75% saturated, d) fully saturated; ..... 63

**Figure 4.3** (i) Pressure and temperature changes during 25 cyclic compressor tests of  $V_{20}Ti_{32}Cr_{48}$  alloy with fully saturated  $H_2$  up to 240°C; (ii) 75 % saturated  $H_2$  up to 260°C; (iii) 50% saturated  $H_2$  up to 260°C and (iv) 0% saturated  $H_2$  up to 260°C..... 64

**Figure 4.4** Cyclic compressor performance comparison of  $V_{20}Ti_{32}Cr_{48}$  alloy with different initial hydrogen content in terms of system pressure variation at low temperature of 32.3°C with no. of cycles. .... 65

**Figure 4.5** XRD profiles of  $V_{20}Ti_{32}Cr_{48}$  alloy before and after compressor cycling with different initial hydrogen content. .... 66

**Figure 4.6** Pressure and temperature changes during 25 cyclic compressor tests of  $V_{20}Ti_{32}Cr_{48}$  alloy with fully saturated  $H_2$  up to (i) 240°C; (ii) 200°C; (iii) 175°C; (iv)150°C and (v) 100°C..... 67

**Figure 4.7** Cyclic compressor performance comparison of  $V_{20}Ti_{32}Cr_{48}$  alloy with fully saturated  $H_2$  hydrogen content at different temperature in terms of system pressure variation at low temperature of 32.3°C with no. of cycles. .... 68

**Figure 4.8** PCI curves of  $V_{20}Ti_{32}Cr_{48}$  alloy with fully saturated  $H_2$  at RT: (a) before; and after 25 hydrogen compressor cycling tests up to high temperatures - (b) up to 240°C; (c) up to 200°C; (d) up to 175°C; (e) up to 150°C and (f) up to 100°C. The starting point was

decided according to same hydrogen content: fully saturated.  
.....69

**Figure 4.9** PCI curves of  $V_{20}Ti_{32}Cr_{48}$  alloy with half saturated  $H_2$  at RT(a) before and after 25 hydrogen compressor cycling tests up to high temperature (b: up to 260°C; c: up to 200°C; d: up to 150°C and e: up to 100°C). The starting point was decided according to same hydrogen content: half saturated..... 70

**Figure 4.10** Pressure and temperature changes during 25 cyclic compressor tests of  $V_{20}Ti_{32}Cr_{48}$  alloy with half saturated  $H_2$  up to (i) 260°C; (ii) 200°C; (iii) 150°C and (iv) 100°C..... 71

**Figure 4.11** Cyclic compressor performance comparison of  $V_{20}Ti_{32}Cr_{48}$  alloy with half saturated  $H_2$  hydrogen content at different temperature in terms of system pressure variation at low temperature of 32.3°C with no. of cycles..... 72

**Figure 4.12** PCI curves of  $V_{20}Ti_{32}Cr_{48}$  alloy with 0% saturated  $H_2$  (solid solution) at RT: (a) before; and after 25 hydrogen compressor cycling tests up to high temperature (b: up to 260°C; c: up to 200°C; d: up to 150°C and e: up to 100°C). The starting point was decided according to same hydrogen content: solid solution..... 73

**Figure 4.13** Pressure and temperature changes during 25 cyclic compressor tests of  $V_{20}Ti_{32}Cr_{48}$  alloy with solid solution  $H_2$  up to (i) 260°C; (ii) 200°C; (iii) 150°C and (iv) 100°C..... 74

**Figure 4.14** Cyclic compressor performance of  $V_{20}Ti_{32}Cr_{48}$  alloy with solid solution in terms of system pressure variation at low temperature of 32.3°C with no. of cycles..... 75

**Figure 4.15** XRD of  $V_{20}Ti_{32}Cr_{48}$  alloy with fully saturated  $H_2$  after 25 hydrogen compressor cycles up to 100 °C, 150 °C, 175 °C, 200 °C

and 240 °C; .....	76
<b>Figure 4.16</b> XRD of V <sub>20</sub> Ti <sub>32</sub> Cr <sub>48</sub> alloy with half saturated H <sub>2</sub> after 25 hydrogen compressor cycles up to 100 °C, 150 °C, 200 °C and 260 °C. ....	77
<b>Figure 4.17</b> XRD of V <sub>20</sub> Ti <sub>32</sub> Cr <sub>48</sub> alloy with solid solution after 25 hydrogen compressor cycles up to 100 °C, 150 °C, 200 °C and 260 °C. ....	78
<b>Figure 4.18</b> SEM morphology of pristine (a and b) and cycled (c and d) sample up to 240 °C with fully saturated H <sub>2</sub> . ....	79
<b>Figure 4.19</b> (a) The achieved max pressure of sample cell at maximum temperature for each hydrogen compressor cycle measurement; (b) the capacity loss of each state with the changes of H content remained in the alloy at high temperature; (c) the capacity loss of each state with max temperature for hydrogen compressor cycle; (d) H content remained in the alloy at achieved max temperature. ....	80
<b>Figure 4.20</b> Illustration of pressure and temperature changes of hydrogen-metal system during thermal driven hydrogen compression process. ....	81

## List of Tables

- Table 4.1** Atomic percentage of elements in  $V_{20}Ti_{32}Cr_{48}$  alloy as determined by EDS analysis. The point no. corresponds to the different positions as shown in Fig. 6 (b) and (d). ..... 82
- Table 4.2** Summary of detailed parameters for hydrogen compressor cycling test for  $V_{20}Ti_{32}Cr_{48}$  alloy at various conditions..... 83



# **1. Introduction**

## **1.1 Hydrogen energy**

Recently, global warming and environmental pollution by the excessive emission of harmful gases such as CO<sub>2</sub>, CO, NO<sub>x</sub> etc. during the usage of nonrenewable fossil fuels and natural gases are urgent problems to be solved. Due to this, the global demand for the development of sustainable energy system became more and more huge. Many kinds of renewable energies, such as: wind power, solar power, ocean energy, biomass energy, geothermal energy as well as hydrogen energy attracted lots of attentions worldwide [1-2]. However, all the options except hydrogen energy, are strongly dependent on either time or region and are available limited to use. Therefore, hydrogen energy has been considered to be the most promising and possible way to solve the above problems because hydrogen offers many advantages such as: high abundance on the earth, easily produced from any kinds of primary energy, highest gravimetric energy density and top of the above, being environmentally friendly owing to its oxidation product as water only [3]. In recent years, hydrogen energy industry all over the world including production, storage and transportation has been developed a lot with the threefold demand for hydrogen. Global spending on hydrogen energy research, development and demonstration

has risen greatly over the past few years. Especially after G20 Summit that was hosted by the Government of Japan in 2019, the hydrogen energy will enjoy unprecedented political and business momentum and will play a key role in a clean, secure and affordable energy future [4].

## 1.2 Hydrogen storage methods

Hydrogen is the first element in the periodic table and has three isotopes: protium (H, 1 proton and 1 electron, atomic weight - 1), deuterium (D, 1 proton, 1 neutron and 1 electron, atomic weight - 2) and tritium (T, 1 proton, 2 neutron and 1 electron, atomic weight - 3). The most often form we used is H because of its abundance on the earth. Various phases of the hydrogen molecule  $H_2$  can be found according to different temperature and pressure conditions. As shown in the phase diagram of hydrogen in Fig. 1.1[5], hydrogen is in a solid state with the density of  $70.6 \text{ kg/m}^3$  below 11K (-262 °C) [5]. At standard temperature and pressure conditions (STP, 273 K and 0.1 MPa pressure), hydrogen molecule is in gaseous form with the low density of  $0.089886 \text{ kg/m}^3$ . At ambient temperature, the hydrogen gas can be described by the van der Waals equation:

$$P = \frac{nRT}{V-nb} - a \frac{n^2}{V^2} , \quad (1.11)$$

where,  $P$  is pressure of the gas,  $n$  is mole numbers,  $R$  is gas constant ( $8.314 \text{ J}\cdot\text{K}^{-1}\cdot\text{mol}^{-1}$ ),  $T$  is absolute temperature,  $V$  is volume of gas,  $b$  is occupied volume by hydrogen

molecules ( $2.66 \times 10^{-5} \text{ m}^3 \cdot \text{mol}^{-1}$ ),  $a$  is interaction constant ( $2.476 \times 10^{-2} \text{ m}^6 \cdot \text{Pa} \cdot \text{mol}^{-2}$ ).

The strong repulsion between hydrogen molecules leads to the critical temperature of 33 K. Liquid hydrogen only exists in a small blue region as shown in Fig 1.[5]. Under the extreme conditions *i.e.* super higher pressure or temperature, the hydrogen molecules may split into hydrogen atoms and rearrange to highly ordered H metal or liquid metal.

It is necessary and crucial to store hydrogen in an efficient approach and improve its volumetric as well as gravimetric density when we use it for mobile and stationary applications. Normally, there are three methods related to three states of hydrogen and usually used for hydrogen storage according to the requirement: storage in compressed state, liquid state and solid state. The next section describes these methods in detail.

### **1.2.1 Storage in compressed state**

Hydrogen storage in compressed state in the cylinder is the most common system that we use for the requirement of small amount of hydrogen with the maximum pressure of 15 MPa, especially for experimental study in laboratory in Japan. It has been reported that the newly developed cylinders made of lightweight composite material could withstand 70 MPa high pressure with a remarkable volumetric density of  $36 \text{ kg} \cdot \text{m}^{-3}$ [5]. However, the gravimetric density for hydrogen storage decreases with the increasing system pressure due to the increasing wall thickness of the cylinder that is required for

the safety consideration. Usually, the following equation is used to calculate the wall thickness of a cylinder's inner and outer hemispheric layers [1].

$$\frac{d\omega}{d\sigma} = \frac{\Delta p}{2\sigma_v + \Delta p} \quad (1.12)$$

Here,  $d\omega$  is the thickness of the cylinder wall,  $d\sigma$  is the outer diameter of the cylinder,  $\Delta p$  is the overpressure and  $\sigma_v$  is the tensile strength of the cylinder wall material. The development of the new materials for hydrogen cylinder should be focused on increasing of the tensile strength and decreasing the materials density at the same time. Different materials for the cylinder wall provide a wide range of tensile strength from 50 MPa for aluminum to 1100 MPa for steel of high quality.

Hydrogen gas can be compressed by using mechanical compressor or metal hydrides based hydrogen compressor. The requirement for hydrogen compressor is strict due to the highly diffusive nature of the hydrogen. From the perspective of theoretical calculation, theoretical work that consumed during isothermal compression can be expressed by the following equation [6]:

$$\Delta G = RT \cdot \ln \left( \frac{P}{P_0} \right), \quad (1.13)$$

where  $R$  is gas constant ( $8.314 \text{ J} \cdot \text{mol}^{-1} \cdot \text{K}^{-1}$ ),  $T$  is absolute temperature and  $P_0$  is initial pressure and  $P$  is final achieved pressure.

The energy consumed during the compression from 0.1 MPa to 70 MPa was

reported as 2.21 kWh/kg [5]. But the actual consumption for hydrogen compression is much higher due to the non-isothermal compression in real cases. The main disadvantage related to compressed hydrogen is limited low storage density and very high gas pressure in the cylinder, which gives lots of uncertain safety problems during practical applications.

### **1.2.2 Storage in liquid state**

Liquid hydrogen can be stored in a cryogenic tank at 21.2 K at ambient pressure with a very high volumetric density of  $70.8 \text{ kg/m}^3$ , slightly higher than  $70.6 \text{ kg/m}^3$  of solid hydrogen. It has been a good option to use liquid hydrogen for space applications due to its highest energy-to-weight ratio. However, the main challenges of hydrogen storage in liquid state are the requirement of huge amount of energy and proper thermal insulation of cryogenic tank to avoid the boiling-off of hydrogen. The boil-off rate of hydrogen in the liquid hydrogen storage container can be controlled by changing its size, shape and thermal insulation. In principle, a sphere shape is the best option for cryogenic tank due to the least surface to volume ratio, which can uniformly distribute the stress and strain. The surface to volume ratio is proportional to boil-off losses caused by heat leaks. The evaporation rate of hydrogen can be reduced greatly with the increase of tank size, however, it leads to the rising of manufacturing expenses for large-sized spherical vessel [1].

Despite the remarkable volumetric density, hydrogen storage in liquid state is not frequently utilized due to the following reasons. Firstly, it requires at least 35% of the total storage hydrogen energy during liquefying processes. Secondly, hydrogen evaporation is very easy during transportation and refueling. Thirdly, it is very easy and quick to be pressurized because liquid hydrogen may always absorb heat from outer environment, which is unwanted for on-board vehicles. All these drawbacks put liquid hydrogen into a dilemma of application.

### **1.2.3 Storage in solid state**

Hydrogen interacts with some metal and alloys to form metal hydrides, leading to solid state storage under ambient temperature and pressure, which gives them the important safety advantage over the former two methods. Metal hydrides have higher energy density than gaseous and liquid hydrogen, for example, in the cases of  $MgH_2$ , the energy density can be reached to 9 MJ/kg (Mg) [5-10].

To be an optimum and potential solid state hydrogen storage candidate, the material is required to contain the following properties:

- 1: High hydrogen storage capacity in volumetric and gravimetric density.
- 2: Suitable thermodynamic properties: reversible hydrogen absorption/desorption at lower / ambient temperature and moderate pressure.

- 3: Fast kinetics: hydrogen absorption/desorption occur within short time.
- 4: High stability against the poisoning due to the traces of O<sub>2</sub> and moisture for long cycle life.
- 5: Good cyclic durability.
- 6: Low cost and abundant in the nature.
- 7: Easy handling and high safety.

Hydrogen storage materials are classified to different types on the basis of their sorption method *i.e.* either physisorption or chemisorption of hydrogen gas [1]. The former type hydrogen storage materials absorb hydrogen mainly in molecular form depending on the larger surface area, which could interact with hydrogen via van der Waals force at lower temperature [11]. This includes carbon based materials, metal organic frameworks, covalent organic frameworks, zeolites, micro porous metal coordination materials, clathrates and nanostructured materials. The amount of absorbed hydrogen is assumed to be proportional to the surface area of the materials, thus the effective way to improve the hydrogen storage capacity of such materials is enlarging the surface area by designing into porous structure. The latter type hydrogen storage materials absorb hydrogen gas by chemically bonded hydride formation, in another word, store hydrogen in atomic state. This allows the significant improvement of volumetric density

that is comparable or even better than compressed hydrogen and liquid hydrogen. The hydrides are classified into two main groups: metal hydrides and non-metals hydrides [5, 11]. The examples of typical metal hydrides are  $\text{LaNi}_5$ ,  $\text{FeTi}$ ,  $\text{V-Ti-Cr}$  etc., while non-metal hydrides are hydrocarbons, boron and nitrogen hydrides. A lot of attention has been given to metal hydrides due to their lower operating temperature and pressure that is suitable for fuel cell vehicles.

### **1.3 Hydrogen absorption/desorption properties of hydrogen storage materials**

#### **1.3.1 Hydrogen absorption/desorption characteristics of hydrogen storage materials**

Typical hydrogen absorption/desorption characteristics of hydrogen storage materials can be described by pressure-composition-isothermal (PCI) measurements as shown in Fig. 1.2 [3], which can be obtained by measuring the hydrogen concentration in the metal alloys as a function of the surrounding hydrogen gas pressure isothermally at equilibrium states. When hydrogen contacts with metal, several steps as shown in Fig. 1.3 takes place. Firstly, hydrogen molecule approach to the surface of metals and be physisorbed through van der Waals interaction. After the dissociation of the hydrogen molecule in to two hydrogen atoms, hydrogen atoms start to penetrate into the host metal,

and gradually occupy the interstitial sites of metal randomly with forming the solid solution in the bulk, which was denoted as  $\alpha$ -phase. In the next, a stable chemically bonded hydride phase, denoted as  $\beta$ -phase, formed between hydrogen atoms and metal along with the alteration in the crystal structure of host metal. The pressure in this process remains constant in the ideal equilibrium conditions even though hydrogen is absorbed continuously due to the Gibbs phase rules. The Gibbs phase rules is described as follows:

$$F = c - p + 2 \quad (1.1)$$

Here,  $F$  represents the degrees of freedom,  $c$  is the total number of components and  $p$  indicates the phases in the system. Under the equilibrium conditions, only hydrogen and metal are involved, the total number of components is 2. Considering that  $\alpha$ -phase,  $\beta$ -phase and gaseous hydrogen phase coexist in the metal, the total phase number is 3. So  $F$  is calculated to be 1, indicating that only one variable parameter can be changed among pressure and hydrogen concentration at a given temperature. Thus, the hydrogen pressure remains constant under isothermal conditions when increasing the hydrogen concentration, which is called the plateau (equilibrium) pressure. With increasing hydrogen concentration, hydrogen in  $\beta$ -phase gets saturated at certain point. The pressure is no more constant at this point but starting to raise vertical asymptotically with further increasing of hydrogen (gas) amount if there is no other related phase formation.

The PCI diagram is the characteristic feature of the hydride forming materials and plays an important role in hydrogen storage application. The plateau width, often regarded as a reversible hydrogen storage capacity of the materials, not only decides how much hydrogen can be stored in the materials, but also greatly affects the hydrogen compression efficiency of hydride materials. A flat plateau with a small slope ensures the reversibility of hydrogen absorption and desorption. The plateau width decreases with the ascending system temperature and vanish completely at critical point  $T_c$  (as shown in Fig. 1.1) accompanying the continuous conversion from  $\alpha$ -phase to  $\beta$ -phase.

In particular, the hydrogen absorption plateau pressure may be slightly different from desorption plateau pressure, which is known as a hysteresis. Hysteresis is another important factor that could significantly affect hydrogen compression performance in the real MH systems [6]. It is caused by the stresses and strains which appeared because of the difference in molar volume between the growth of metal hydride nuclei and the hydride forming materials matrix.

Thus, the above two factors' influence on the performance of MH hydrogen compressors cannot be ignored when utilizing the materials for hydrogen storage and hydrogen compression due to their strong effect on the cyclic durability and efficiency. The details will be discussed in section 1.5.

### 1.3.2 Thermodynamics of hydrogen storage

The applications of metal hydrides for hydrogen storage and hydrogen compression, are based on the reversible heat-driven interaction of hydrogen storage materials with hydrogen gas, as expressed in following equation:



where,  $M$  is a metal/alloy or other materials that can absorb/desorb hydrogen,  $s$  and  $g$  denote the solid and gaseous phases, respectively. The hydrogen gas reacts with the metal and forms metal hydride exothermically with the release of heat ( $Q > 0$ ) during the absorption process. For the reverse reaction, the hydride releases hydrogen gas when the same amount of exothermic heat during the hydrogenation is supplied to the hydride.

Based on the reaction 1.2, the Gibbs's free energy of the whole system can be expressed in terms of the total enthalpy changes  $\Delta H$  and entropy change  $\Delta S$  of each component as follows:

$$\Delta G = \Delta H - T\Delta S \quad (1.3)$$

At equilibrium condition,  $\Delta G$  is considered to be zero, so eq. 1.3 can be expressed as:

$$\Delta H = T\Delta S \quad (1.4)$$

Here, 
$$\Delta S = S_{MH_2} - S_{H_2} - S_M \quad (1.5)$$

Since the difference between the entropy of the solid metal hydride and metal is very

small, the value of  $S_{MH2}-S_M$  is quite negligible when comparing with the entropy of the hydrogen gas. Thus

$$\Delta S \approx -S_{H2} \quad (1.6)$$

For H<sub>2</sub> gas,

$$S_{H2} = S_{H2}^0 - R \ln \frac{P^{eq}}{P_0} \quad (1.7)$$

So

$$\Delta S = S_{MH2} - (S_{H2}^0 - R \ln \frac{P^{eq}}{P_0}) - S_M \quad (1.8)$$

$$\Delta S = \Delta S^0 + R \ln \frac{P^{eq}}{P_0} \quad (1.9)$$

On combining equation (1.4) and (1.9), it can be written as:

$$\ln \frac{P^{eq}}{P_0} = \frac{\Delta H}{RT} - \frac{\Delta S^0}{R}, \quad (1.10)$$

where  $P_0 = 1 \text{ atm} = 1.013 \text{ bar} = 0.1 \text{ MPa}$ .  $R$  is the gas constant:  $8.314 \text{ J}/(\text{mol} \cdot \text{K})$ . This is known as the van't Hoff equation. This is a straight line equation which can be used to calculate  $\frac{\Delta H}{R}$  and  $-\frac{\Delta S^0}{R}$  from the slope and intercept respectively by plotting  $\ln(P^{eq}/P^0)$  versus  $1/T$  curve using the experimental absorption/desorption plateau pressures at different temperatures. This relationship can be applied over a wide temperature range and is useful to predict the hydrogen absorption/desorption equilibrium pressure at any temperature.

## **1.4 Hydrogen storage alloys developed for hydrogen compression**

Alloys having general formula of  $A_xB_y$  are prior option for hydrogen storage/compression, where A is the metal which could form a stable hydride with hydrogen, B is the metal that has less affinity to hydrogen. In the next section, four types of alloys will be described in details.

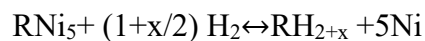
### **1.4.1 $AB_5$ type alloys**

$AB_5$  types alloys where A is rare earth metal and B is mainly Ni, satisfy the requirement for the hydrogen compression materials *i.e.* they are easy to activate, capable to absorb/desorb hydrogen at mild temperature and pressure conditions, have fast kinetics for charge/discharge of hydrogen, flat plateau and narrow hysteresis. These alloys have been intensively investigated for hydrogen compressor applications, allowing the changes of the absorption pressure from 0.1MPa to 2-3 MPa at 25 °C, and the desorption pressure from 1.5-2 MPa to 20 MPa in the temperature range of 100 °C to 150 °C [5, 12, 13].

A typical and well-known example of this family is  $LaNi_5$  with  $CaCu_5$ -type hexagonal structure. It has excellent hydrogen storage properties at room temperature but the disadvantages associated with it are expensive cost, lower plateau pressure and bad cyclic durability during continuous hydrogen absorption/desorption processes [14, 15]. A

lot of efforts have been put in to improve its performance. Substitution of different element in LaNi<sub>5</sub> alloys could vary the suction and discharge pressure. When La is substituted by Ce, Mm (mischmetal), Ca or Y, the plateau pressure can be increased, however, when Ni is substituted by Sn, Al or Mn, the plateau pressure decreases [16-22]. The substitution of different elements could greatly affect the thermodynamic properties of these alloys.

The big issue restricting the application of AB<sub>5</sub> type alloy for hydrogen compressor is the performance deterioration during long cycles of charge/discharge with continuous decay of hydrogen storage capacity, increasing slope and large hysteresis [5, 15, 23-24]. One important reason is the occurrence of thermodynamically favorable disproportionation reaction [15, 25-34]. As an example, in the case of RNi<sub>5</sub>, it can be expressed as follows:



Experimental studies revealed that not only the disproportionation reaction but also the structural changes lead to the hydrogen storage performance deterioration. The appearance of lattice strains [29-31, 35], the formation of defects [22, 30, 35] as well as the poisoning effects by the traces of impurity gases [32] could be the possible reason for this phenomenon.

A lot of AB<sub>5</sub>-type alloys based hydrogen compressor system have been developed so far. MmNi<sub>4.25</sub>Al<sub>0.75</sub> was reported by Esquivel's group for the utilization as one-stage thermal hydrogen compression with a compression ratio of 5.7 in the temperature range of 25°C – 80 °C [36]. A tuned dual stage hydrogen compressor with improved compression ratio was constructed using LaNi<sub>5</sub> in the first stage and Ca<sub>0.2</sub>Mm<sub>0.8</sub>Ni<sub>5</sub> in the second stage [37].

Another combination of LaNi<sub>5</sub> and La<sub>0.35</sub>Ce<sub>0.45</sub>Ca<sub>0.2</sub>Ni<sub>4.95</sub>Al<sub>0.05</sub> in double-stage metal hydride-based heat transformer have been investigated with the maximum compression ratio of 22 at 140 °C with 0.2 MPa supply pressure [38]. Similarly, La<sub>0.35</sub>Ce<sub>0.45</sub>Ca<sub>0.2</sub>Ni<sub>4.95</sub>Al<sub>0.05</sub> alloy was also developed as the first stage hydrogen compression alloy in Chen's work [39], which helped to construct 70 MPa metal hydride hydrogen compressor. Comparable hydrogen storage performance of two stage alloy for hydrogen compression via LaNi<sub>5</sub> and La<sub>0.5</sub>Ce<sub>0.5</sub>Ni<sub>5</sub> were investigated for 18180 hydrogen compression cycles [40].

### **1.4.2 AB<sub>2</sub> type alloys**

AB<sub>2</sub> type alloys with laves phases are also attractive as potential hydrogen storage materials with covering much broader ranges of the operation pressure from 10<sup>-4</sup> Pa to dozens of MPa. There are three types crystal structure among them: hexagonal C14

(MgCu<sub>2</sub> and ZrMn<sub>2</sub>), cubic C15 (ZrV<sub>2</sub> and MgZn<sub>2</sub>), and double hexagonal C36 (MgNi<sub>2</sub>).

There are two factors that can affect the structural stability of the Laves phase alloys:

1. The electronic factor that can be controlled by the valence and electronegativity of the elements.
2. The geometric factor (two elements atomic radii ratio).

The advantage of the Laves phase is their relatively high capacity to store hydrogen with faster kinetics and good cycle life. However, the formation of stable hydrides makes it difficult to release hydrogen at room temperature, which is the disadvantage of them. The thermodynamic and electrochemical properties can be improved by substitution of different element in a certain amount [41]. For example, the system of Zr<sub>1-x</sub>T<sub>x</sub>(Mn, Cr)<sub>2-y</sub>M<sub>y</sub>(T = Nb, Y, Hf, Sc, Ti and M = Ge, Cu, Ni, Al, Si, V) was studied extensively by many researchers [42].

AB<sub>2</sub> type alloys were reported as a good candidate used especially for second stage of multi-stage hydrogen compressor due to the higher plateau pressure than other type alloys at same operation temperature. In 2018, Ti<sub>1.1</sub>CrMn was reported by our group that can be worked as second stage alloy and 82 MPa hydrogen pressure could be achieved upon being heated to 200 °C [43]. This alloy showed good cyclic durability under 100 cycles of hydrogen compression.

### 1.4.3 AB type alloys

TiFe is a representative alloy of AB type alloys family, in which A and B element are arranged regularly. Intermetallic TiFe has BCC type crystal structure. It is a potential candidate for hydrogen storage applications because of the inexpensive price of both the elements, the reversibility of hydrogen absorption and desorption at room temperature with 1.9 wt% reversible capacity [44].

However, TiFe has some drawbacks when put it into application [45-47]: the stable oxidation layer on the surface makes it more difficult to activate. Two plateaus are formed during hydrogenation process corresponding to the formation of two stable phases,  $\beta$ -phase and  $\gamma$ -phase. In addition, high hysteresis causes lower hydrogen compression ratio. Moreover, its high sensitivity to the presence of trace O<sub>2</sub> and moisture result in the formation of fast inactivated state.

In order to improve the hydrogen storage performance of TiFe alloy, substitution with other elements was considered. It was reported that the replacement of Fe with Cr, Ni, Mn V or Co could be beneficial to absorption process [48-54]. Besides, the variations of sample preparation and treatment such as high-pressure torsion (HPT) [55-56], groove rolling (GR) [57] and ball milling with different organic additives [58-60] were also

proved to be effective ways to activate TiFe alloy before the usage for hydrogen storage.

#### 1.4.4 BCC type alloys

Vanadium based BCC-alloys have been extensively considered for MH compressors worldwide due to their excellent features *i.e.* high hydrogen storage capacity (4 wt%), fast kinetics for hydrogen ab/desorption at ambient temperature [2,61-67]. Nevertheless, it is still a challenge to employ these alloys for practical applications owing to difficult activation, pulverization, and bad cyclic behaviors [61,68,69]. Moreover, V element is relatively expensive, which makes it difficult to be employed from economic point of view. Addition of alloying elements such as Ti, Cr, Fe, Co, Mo etc. could resolve all these issues significantly [61,62,68,69].

Although the hydrogen storage properties and cyclic durability of several BCC alloys were investigated sufficiently at mild conditions [70-71], the performance under extreme conditions for hydrogen compression application was evaluated seldomly until now. For hydrogen compression cycling test, the actual operation condition and cyclic durability are key issues when put it to the practical applications [6]. Recently, the cyclic performance of hydrogen ab/desorption of two different V-Ti-Cr alloys, namely  $V_{40}Ti_{21.5}Cr_{38.5}$  and  $V_{20}Ti_{32}Cr_{48}$  were systematically investigated for 100 cycles with a variation from the lower pressure (2 MPa for  $V_{40}Ti_{21.5}Cr_{38.5}$  and 0.07 MPa for  $V_{20}Ti_{32}Cr_{48}$ )

at room temperature to higher discharge pressure of 20 MPa at high temperature (160 °C for  $V_{40}Ti_{21.5}Cr_{38.5}$  and 310 °C for  $V_{20}Ti_{32}Cr_{48}$  ) by our group [72]. The former one was found stable for cyclic hydrogen storage properties after losing 22% hydrogen storage capacity in initial ten compression cycles, whereas the hydrogen storage capacity of the other alloy was decreased continuously due to the formation of thermodynamically stable monohydride phases of V and Ti [72]. In spite of disproportionation and degradation,  $V_{20}Ti_{32}Cr_{48}$  alloys still have larger potential to be used because of comparatively larger hydrogen storage capacity than the first one after 10 compressor cycles. In addition, lower V content of  $V_{20}Ti_{32}Cr_{48}$  alloy with cheaper price has a relevant low plateau pressure, which can achieve first stage compression easily with larger hydrogen compression ratio. Due to above reasons, this alloy was chosen in this study as a model system to know the suitable operating conditions for hydrogen compression without disproportionation and degradation.

## **1.5 Recent development of hydrogen compressor**

Hydrogen storage has been used for industrial development in recent years. Hydrogen compression is an important technology for hydrogen transportation and usage. Not only the hydrogen station but also hydrogen storage tank for on board application needs this crucial supporting process in order to supply hydrogen after running out of

them. In this section, the comparison between traditional mechanical compressor and metal hydrides based hydrogen compressor will be made to better understand the important role that metal hydrides based hydrogen compressor played. Then the recent development of hydrogen compressor will be briefly introduced.

Nowadays, traditional mechanical compressor has been used for the compression of hydrogen gas in commercially available fuel cell vehicles. However, it has many problems: too noisy during usage, costly, easy hydrogen embrittlement of the driving parts [61]. To solve this problem, hydrogen compression based on the reversible thermal energy-driven interaction of hydrogen storage materials with hydrogen gas has been developed as a promising option for hydrogen energy systems [5]. It works only by absorbing H<sub>2</sub> by hydride forming metals and alloys at ambient temperature and releasing pure H<sub>2</sub> when increasing the system temperature.

According to the industrial requirement of durable cycling stability and high efficiency, the hydride forming metals and alloys should satisfy the following performance features: considerable reversible hydrogen storage capacity, good hydrogen compression ratio from nice PCI properties, easy and fast hydrogenation/dehydrogenation at ambient temperature and pressure, flat plateau and narrow hysteresis as well as easier pretreatment and activation with less cost [5, 73]. Most importantly, the materials should

have a good cyclic durability at extremely high temperature as well as pressure conditions and should be stable enough to be not deteriorated.

There are lots of reports related to MH hydrogen compressors in numerous scientific papers, patents since last century. In 1973, a hydrides compressor used for hydrogen refrigerator through  $\text{LaNi}_5$  alloy was developed by Vanmal, which could compress the hydrogen from 0.4 MPa to 4.5 MPa [74]. It was reported by Silva that TiFe based hydrogen compressor for industrial prototype desorbed 10MPa hydrogen at 250 °C [75]. A two stage hydrogen compressor designed by Shmal'ko et al. could pressurize the hydrogen into 15 MPa through  $\text{LaNi}_{4.5}\text{Mn}_{0.5}$  alloy in 'low temperature' part and  $\text{LaNi}_5$  in 'high temperature' part respectively [76]. A six-stage hydride compressor, created by one American company Ergenics, had the ability to compress hydrogen from normal atmospheric pressure to 21 MPa [77]. Three  $\text{AB}_5$  type alloys of  $\text{LaNi}_{4.8}\text{Sn}_{0.2}$ ,  $\text{LaNi}_5$  and  $\text{MmNi}_{4.7}\text{Al}_{0.3}$  were used for a three-stage metal hydride hydrogen compressor by Laurencelle et al. in 2009, the system produces 2.3 MPa hydrogen in a temperature range of 20 to 80 °C [78]. Similar hydrogen compressor constructions were carried out by Cieslik et al., Popeneciu et al., Kim et al. and Muthukumar et al. with achieved hydrogen pressure less than 10 MPa [79-81]. Dramatically higher pressure could be achieved using a dual-stage hydrogen compressor developed by Chen et al. in 2010 [39]. They built a

74.5 MPa double-stage metal hydride hydrogen compressor by using La–Ce–Ca–Ni–Al (AB<sub>5</sub> type) and Ti–Zr–Cr–Fe–V (AB<sub>2</sub> type) multicomponent alloys with hydrogen compression capacity of around 2000 L/cycle and the hydrogen flow rate of the compressor around 34.6 L/min [39]. Further improvement in hydrogen compression pressure up to 82 MPa was achieved by our group in the leadership of Ichikawa in 2018. Ti<sub>1.1</sub>CrMn was used as the working alloy and such a high pressure was attained by heating the system to 200 °C. 100 cycles of hydrogen compression test revealed high cyclic durability of the above sample [43].

Although many experiments and investigations were conducted to build a hydrogen compressor with higher and higher pressure, the issues of the cyclic durability of hydrogen storage materials for continuous usage, the cost for construction, maintenance and the safety should be further considered to enable clean hydrogen to fulfil its long-term potential.

# Figures

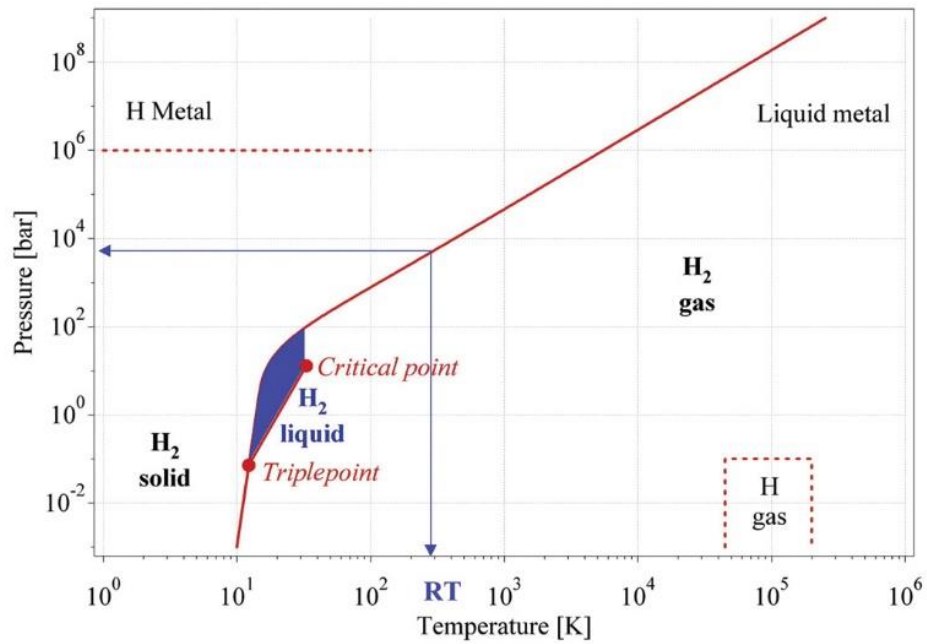


**Figure 1.1 Primitive phase diagram of hydrogen under different temperature and pressure conditions [1].**

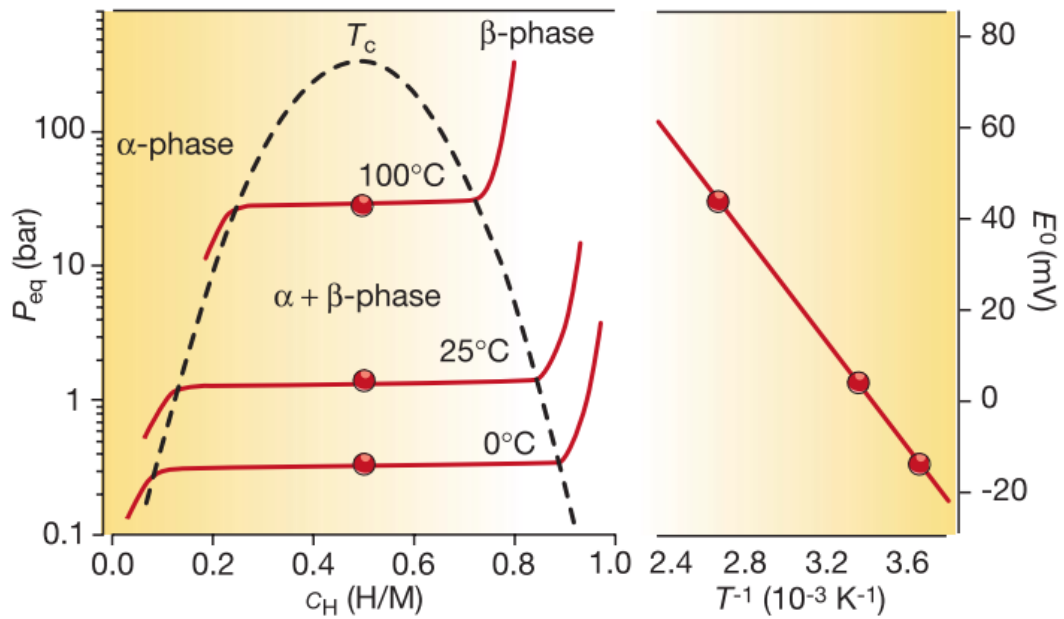


**Figure 1.2: Pressure-composition-isothermal (PCI) measurements and a Van't Hoff curve (logarithm of the plateau pressure against the reciprocal temperature); values are for LaNi<sub>5</sub> [3].**

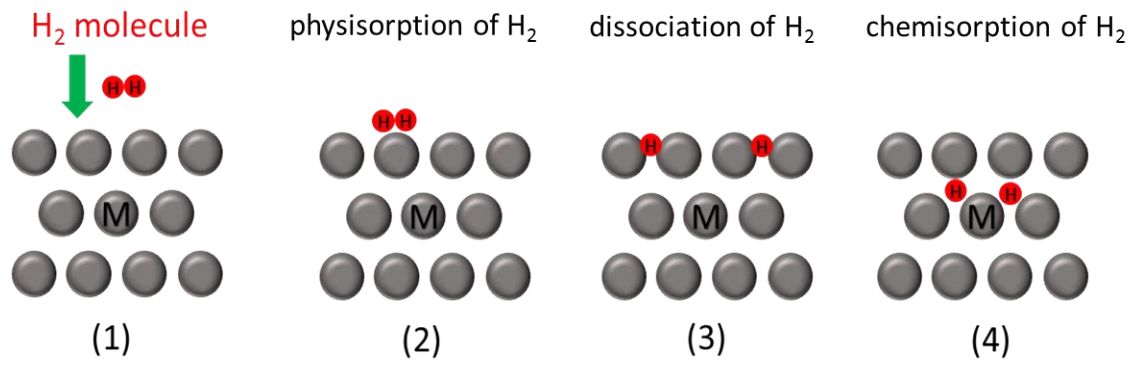


**Figure 1.3 Illustration of the procedure of hydrogen gas reacting with metal alloys.**

## 2. Purpose of this thesis

Hydrogen energy has been considered to be a clean, secure and affordable energy system, which could greatly help the human being to solve the global warming and energy exhausting problems. Hydrogen compression plays a crucial role in the process of hydrogen energy industrial development. Metal hydrides based hydrogen compression has been proved to be a good candidate over traditional mechanical compression of hydrogen and attracted attentions of many researchers worldwide. Many efforts from all over the world's researchers have been put in to find the suitable hydrogen compression material from different categories of hydride. However, most of the works have been focused only on the hydrogenation properties at ambient conditions or the cyclic compressor properties from practical point of view. Several reports have shown the disproportionation in the alloy, resulting in the degradation of compressor performance with number of cycles. However, no work has focused to identify the critical conditions for temperature and pressure, where the alloys can work without disproportionation and performance degradation. As discussed above,  $V_{20}Ti_{32}Cr_{48}$  can be a good candidate for hydrogen compressor but it was found to be degraded during 100 thermal hydrogen compressor cycles. Since, no information about the boundary conditions of temperature and pressure for this phenomenon has been investigated, this motivated us to choose

$V_{20}Ti_{32}Cr_{48}$  as a model system in this work to know the suitable conditions to operate this alloy for hydrogen compression without disproportionation and degradation.

In this thesis, two important parameters, hydrogen content in the alloy and the temperature of operation as compressor, have been selected to define the critical conditions for suppressing degradation.

To investigate the hydrogen content influence, the following aspects have been considered and investigated in this thesis. The  $V_{20}Ti_{32}Cr_{48}$  alloy with fixed weight was filled with different amount of hydrogen via precisely controlling of PCI curves. The 25 cycles of hydrogen compressor tests were performed up to a fixed temperature. The hydrogen storage properties were systematically investigated. Structure and morphology information were evaluated to better understand the reason for the disproportion and degradation phenomenon.

Temperature effects for the cyclic properties were also investigated and presented in this thesis. Several different achieved maximum temperatures were set to evaluate  $V_{20}Ti_{32}Cr_{48}$  alloy's hydrogen storage behavior before and after 25 hydrogen compressor cycles. Supportive information about structure and morphology were provided to explain the different hydrogen sorption properties at different temperature.

In the end, the temperature and hydrogen content influence on hydrogen

compressor cyclic durability of  $V_{20}Ti_{32}Cr_{48}$  alloy were comprehensively considered by analyzing the disproportionated and non-disproportionated points. A clear boundary has been identified and presented herein. It will be helpful to guide us about the operating conditions of this alloy for hydrogen compression without disproportionation and degradation. As a general outcome of this thesis, the case study of  $V_{20}Ti_{32}Cr_{48}$  alloy at different extreme conditions would be helpful to generalize this method to all the other hydrogen storage alloys to define their critical conditions without disproportionation and degradation.

## **3. Experimental**

### **3.1 Sample preparation**

$V_{20}Ti_{32}Cr_{48}$  alloy was purchased from Japan metals and chemicals Co Ltd. According to our requirements, the alloy was prepared by arc melting of the starting metals with the respective molar ratio and followed by annealing to dissolve the minor phases. The sample was annealed at 1500 K for 1 hour with the heating rate of 200 K/hr. After second heating treatment at 1673 K for 30 minutes, the sample was cooled down in the furnace under Ar atmosphere. Then a hydrogen pulverization process was performed: evacuate the sample at 400 °C and fill 1.5 MPa hydrogen gas at room temperature, a final evacuation was conducted to remove the absorbed hydrogen gas at 400 °C. Slight pulverization was conducted to get small and fine alloy particles.

### **3.2 Activation process**

Since oxide layer formed in the alloy surface may stop the hydrogen diffusion into the metal alloy, an activation process is necessary to activate the alloy before hydrogen absorption and desorption cycles. For  $V_{20}Ti_{32}Cr_{48}$  alloy, an activation process was performed according to the following steps:

First, the alloy was evacuated and heated from room temperature to 200 °C with the heating rate of 5 °C /min for 2 hours under dynamic vacuum. Secondly, 2 MPa  $H_2$  gas

was filled into this sample cell at 200 °C and was cooled down to room temperature. Then, evacuation was conducted again at 200 °C for 2 hours to completely remove the absorbed H<sub>2</sub> gas. The above process was repeated for 3 times in order to ensure the complete activation of V<sub>20</sub>Ti<sub>32</sub>Cr<sub>48</sub> alloy.

### **3.3 X-ray diffraction (XRD)**

#### **(1) Basic principle**

Powder X-ray diffraction (XRD) is a useful and important technique for the fingerprint of periodic atomic arrangements in a given crystalline material. It provides us a very useful method to identify phase information, measuring crystalline structure and obtaining the lattice parameters, such as average grain size, crystallinity, strain, and crystal defects.

It is known that the atoms in a crystalline materials are arranged periodically and create different sets of lattice planes, where the lattice plane can be described by the Miller indices (*hkl*). As shown in Fig. 3.1, the distance between two adjacent parallel planes, *P*<sub>1</sub> and *P*<sub>2</sub>, is denoted by *d*. The parallel incident X-ray beams are interacted with atoms and reflected by them in a set of parallel beams, which travel through a different optical path with a path difference of  $2d\sin\theta$ . Constructive interference happens when two reflected beams are in-phase or in other words, the path difference between them is an integer

multiple of wavelength. According to this condition, the following equation will be formed:

$$n\lambda = 2d\sin\theta \quad (3.1)$$

Equation (3.1) is known as Bragg's law and provides a simplistic model to understand what conditions are required for diffraction. By varying the diffraction angle  $2\theta$ , we can get different X-ray peaks from the distinctive lattice planes.

## **(2) Measurement procedure**

In this study, X-ray diffraction (XRD) with Rigaku-RINT 2500 (shown in Fig 3.2 (a)) was used to identify the phases and structural changes. This equipment uses the X-ray source of Cu-K $\alpha$  ( $\lambda=1.54 \text{ \AA}$ ) radiation and the energy power of 40 kV and 200 mA. The sample was transferred to the glove box for preparation the XRD plate. To prevent the oxidation from the air and moisture, the sample was kept in a glass plate and covered by a polyimide sheet (thickness  $8\mu\text{m}$ , and produced by Du Pont-Toray Co. Ltd, Kapton) during measurement (as shown in Fig 3.2 (b)).

## **3.4 Scanning electron microscopy (SEM)**

### **(1) Basic principle**

Scanning Electron Microscopy (SEM) uses a focused beam of electrons with high energy to produce signals with magnification of 30000 times at the surface of the solid

samples. The signals reveal information about the sample including the chemical composition and surface morphology.

In principle, the incident high energy electron beam interacts with the sample and generates many signals composing of secondly electrons (SE), back-scattered electrons (BSE), elastically and in-elastically scattered electrons, transmitted electron and X-rays (shown in Fig.3.3(a)). SEM technique uses the signals mainly come from secondly electrons and back-scattered electrons. The generation of secondary electron originates from the repelled specimen electrons by the positively charged electron beam. The great repulsion pushes the specimen electrons out of the atoms. The secondary electrons pose very small energy and only those generated at near surface region can be detected, which leads to the very sensitive nature of secondary electrons to the surface morphology and topography. However, the primary electron beam is scattered when they hits the atomic nuclei and becomes backscattered electrons that holds high energy level and with diverted path. To obtain a BSE image, a detector must be placed in their path. Since different elements have different sized nuclei, more backscattered electrons can be generated from the bigger atom nuclei and that creates different contrast from different elements/phases. By using BSE image, illustrating contrasts in composition in multiphase samples can be obtained.

During the SEM measurement, a charging effect cannot be ignored because of the conductivity difference of various samples. This effect arose from the accumulation of static electric charges on the non-conducting sample surface and deteriorate the SEM image quality. To eliminate this charging effect, coating the non-conducting samples with a thin conductive carbon film and using low vacuum are frequently used methods.

## **(2) Measurement procedure**

Scanning Electron Microscopy (JEOL, JIB-4600F/HKD) was used to get the morphology information of the alloy samples in this work. The sample was spread on the carbon tape that was stuck on the SEM transfer vessel and then covered by the polyimide film as shown in Fig 3.2 (b) (thickness 8 $\mu$ m, and produced by Du Pont-Toray Co. Ltd, Kapton) in order to protect this sample from the air. The polyimide film was removed insider the chamber before performing SEM measurement. 10 kV acceleration voltage was fixed during measurement.

## **3.5 Energy dispersive X-ray spectroscopy (EDS)**

### **(1) Basic principle**

Energy dispersive X-ray spectroscopy (EDS), also called energy dispersive X-ray analysis (EDXA), is a standard method for identifying and quantifying the elements and compositions in the specimen sample. This technique could give us sufficient information

by point, linear, and 2D elemental mapping.

The electrons of the atom in discrete energy levels are bound to the nucleus at ground state (unexcited state) (shown in Fig.3.4 [82]). When a beam of X-ray is focused into the studied sample, the electrons in the inner shell may be excited and eject from the shell while leave an electron hole. To achieve a stable state, the electrons from higher energy levels in the outer shell occupy this electrons hole by releasing energy in the forms of X-ray. The energy and the number of emitted X-rays can be tracked by an energy dispersive spectrometer. As every atom has its own atomic structure with characteristic energy between two shells, that makes it possible to check the elemental composition of the specimen sample by using this technique.

## **(2) Measurement procedure**

In this work, the composition of pristine and cycled  $V_{20}Ti_{32}Cr_{48}$  alloy was checked by Energy dispersive X-ray equipment (EMAX-7000) at the same time of SEM measuring. Point analysis was used to track the composition changes of each sample.

## **3.6 Pressure composition isotherm measurement (PCI)**

### **(1) Basic principle**

Pressure-Composition Isotherms (PCI) or Pressure-Composition Temperature (PCT) is one of the most used sorption measurements to describe the hydride formation

from gaseous hydrogen in the thermodynamics point view [82-83]. It records the hydrogen gas concentration with the changes of surrounding gas pressure at equilibrium conditions isothermally. These measurements can be conducted using either direct volumetric measurements by utilizing a Sievert apparatus or direct gravimetric measurements. Pressure difference drives the absorption and desorption in volumetric measurement. Gravimetric measurements are performed by measuring the weight changes of the sample under isobaric conditions. By comparison, volumetric measurement has a simpler design and cheaper price than gravimetric methods. Gravimetric measurement has some limitation in terms of maximum pressure that is usually limited up to 2 MPa, whereas, volumetric measurement can be used up to 20 MPa [82].

In this work, Sievert's type volumetric measurement (shown in Fig. 3.5 (a)) was used for the evaluation of hydrogen storage behavior of  $V_{20}Ti_{32}Cr_{48}$  alloy at room temperature. Fig. 3.5 (b) shows the schematic illustration for this system. It consists of a gas cylinder, a reservoir and a reactor as well as the connecting line tubes. The volume of the reservoir is denoted as  $V_d$  and is a system parameter with known volume of 75.113  $cm^3$ . The volume of reactor  $V_R$  and line volume  $V_L$  were measured by blank PCI measurement. To determine the absorbing and desorbing amount of hydrogen, the system

parameters were recorded precisely according to each condition.

At initial stage, the hydrogen gas was first filled into the reservoir with certain stabilization time. The total hydrogen amount contained in the system was calculated according to the following expression:

$$N = \left\{ \frac{P_d V_d}{R Z_d T_d} + \frac{P_l V_l}{R Z_l T_l} + \frac{P_r V_r}{R Z_r T_r} \right\} \quad (3.2)$$

Here, mole of hydrogen gas  $N$ , pressure  $P$ , volume  $V$ , temperature  $T$  and compression factor of hydrogen gas  $Z$  with their subscript  $d$ ,  $l$  and  $r$  denote the reservoir, line and reactor, respectively.

After opening the valve existed between the reservoir and reactor, the alloy sample absorb/desorb certain amount of hydrogen which causes the pressure change of the system until it reaches an equilibrium state. In this way, the remained hydrogen gas in the system  $N'$  will be expressed as:

$$N' = \left\{ \frac{P'_d V'_d}{R Z'_d T'_d} + \frac{P'_l V'_l}{R Z'_l T'_l} + \frac{P'_r V'_r}{R Z'_r T'_r} \right\} \quad (3.3)$$

So the total absorbing/desorbing hydrogen gas in weight percentage will be given as:

$$\Delta W = \frac{MH}{MM} * 100\% = \frac{(N-N')*2.016}{M} * 100\% \text{ (wt\%)} \quad (3.4)$$

Once one set of pressure and composition data is recorded, the system gradually increase/decrease the pressure up to the desired set point.

## **(2) Measurement procedure**

The sample holder with activated alloy was connected with the Sievert's type apparatus (Suzuki Shokan Co. Ltd) through a quick connection part as shown in Fig. 3.5(a). Fig. 3.5 (b) shows the schematic illustration of the PCI measurement system. It was made up by gas cylinder, reservoir, reactor, vacuum pump, lines and recording system. Three times H<sub>2</sub> gas purging was conducted to clean the system line. The pressure composition isotherm measurements were performed in the pressure range of 0.001 MPa -7 MPa at room temperature. The reservoir volume was 75.113 cm<sup>3</sup>. The reactor volume and line volume were measured by blank measurement for every sample holder. Because of the swelling of the sample holders after several thermal compression cycles, these were changed from time to time when the swelling was observed.

## **3.7 Hydrogen compressor cycle system**

Hydrogen compressor is a system that can compress hydrogen gas only by thermally driven reversible reaction of metal hydrides. This system with metal hydrides can absorb large amount of hydrogen gas at lower temperature and ambient pressure, then release higher pressure of hydrogen gas only by heating process. It possesses a lot of advantages over traditional mechanical compressors that are simplicity in design and operation, compactness, safety, reliability and absence of mechanical moving parts.

A closed sample cell was filled with certain amount of pure hydrogen gas according to the PCI curves (the starting point of desorption plateau pressure). The hydrogen compressor cycling test was performed using our homemade compressor system as shown in Fig.3.6. The system was heated to different temperatures with the fixed heating rate of 5 °C/min using a digital heater, followed by cooling down to room temperature. This process was treated as one cycle and repeated for 25 times at each condition. A pressure gauge and a thermometer were connected to the sample cell with a recording system, which can record the pressure and temperature variations during each experiment.

## Figures

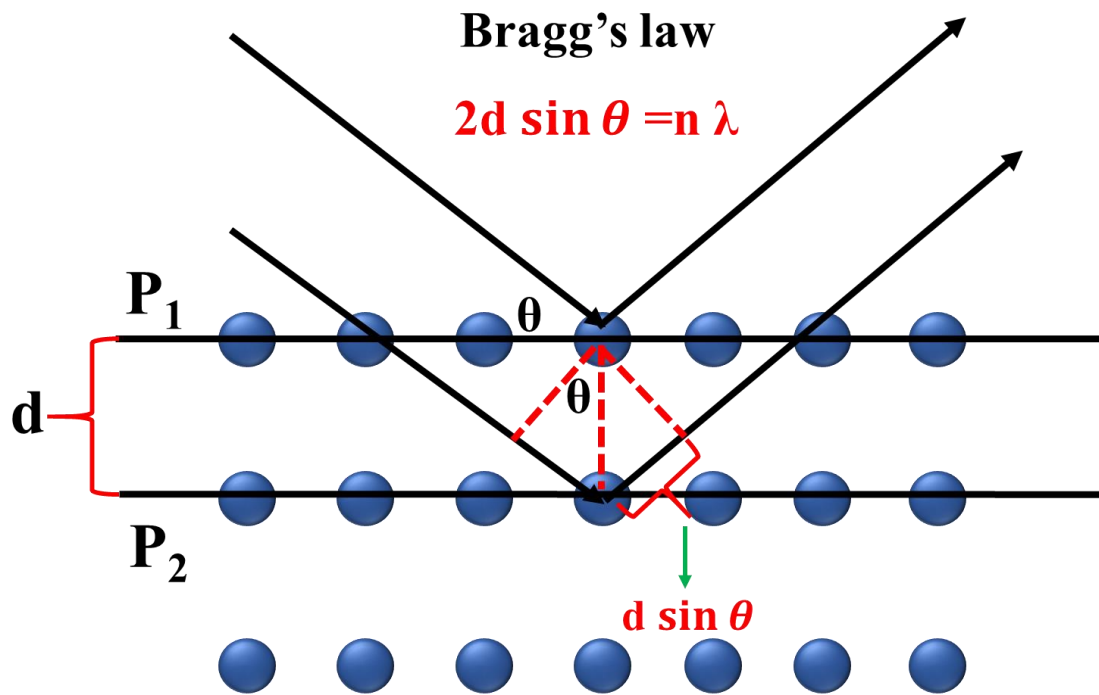
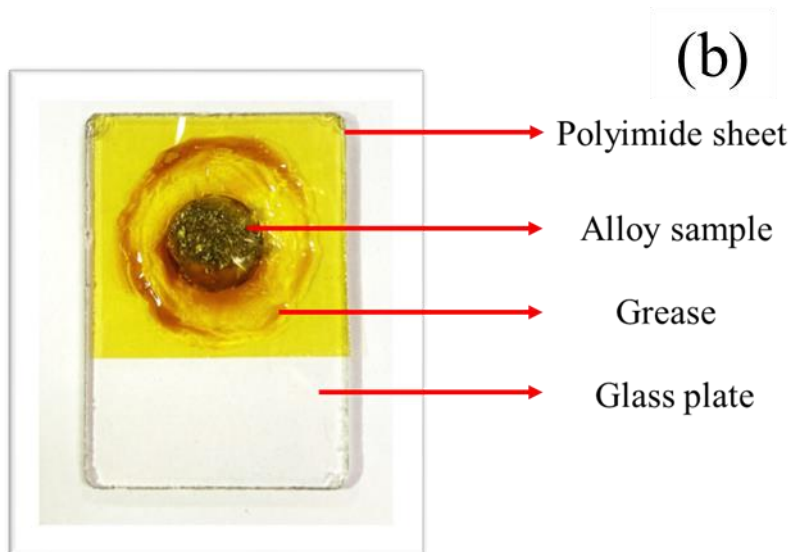
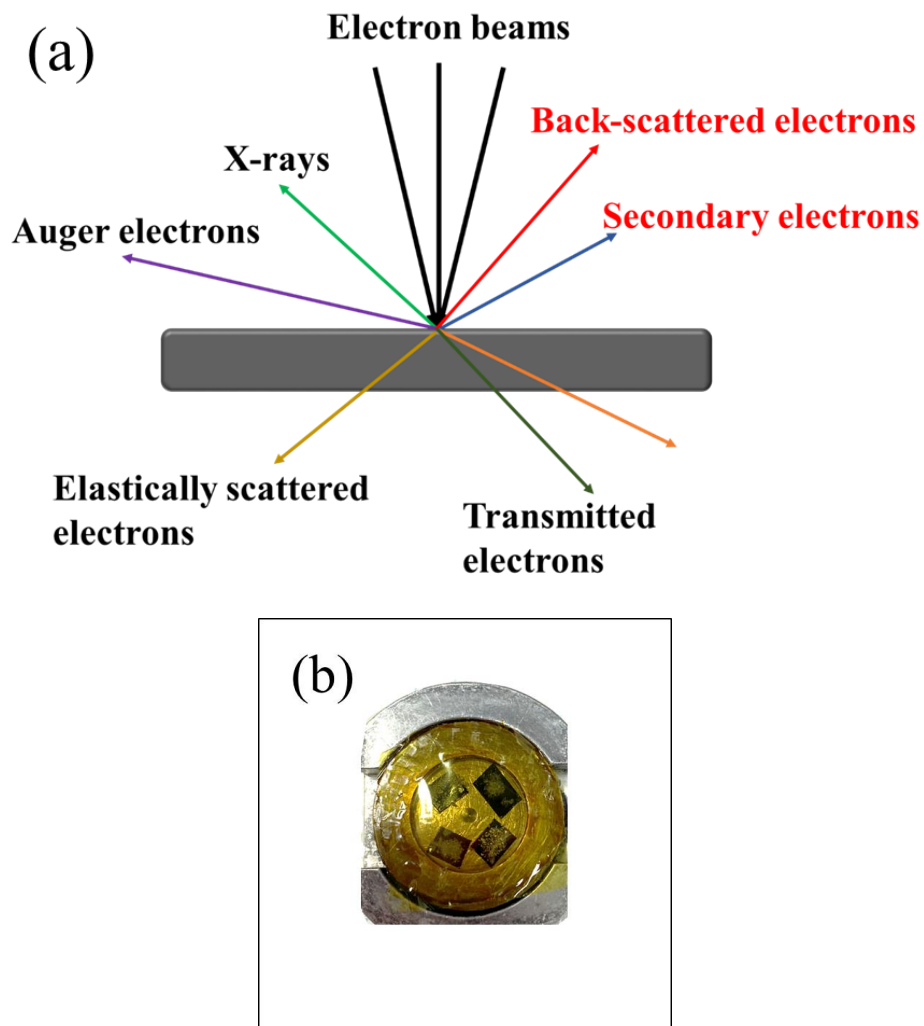


Figure 3.1: Schematic representation of the diffraction of X-rays from crystal planes.



**Figure 3.2: (a) Rigaku-RINT 2500 X-ray diffraction equipment used in this work, (b) sample plate for XRD.**



**Figure 3.3: (a) Interaction between the incident electron beams with the material, (b) sample plate for SEM-EDS.**

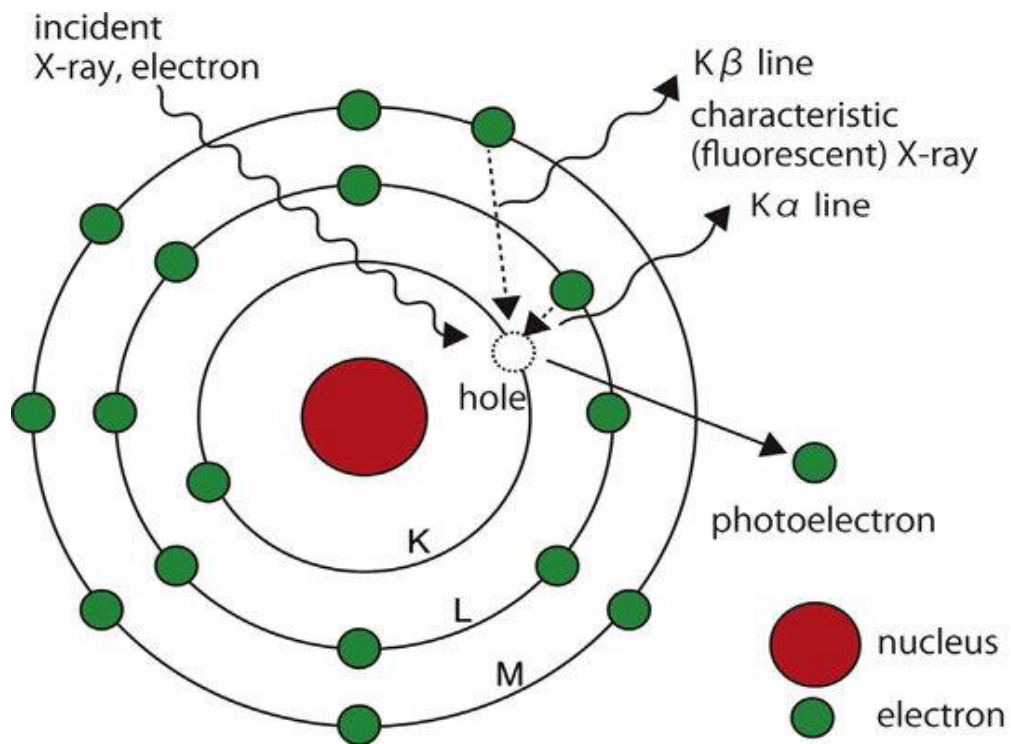


**Figure 3.4: Diagram of generation of characteristic X-ray**

[82].

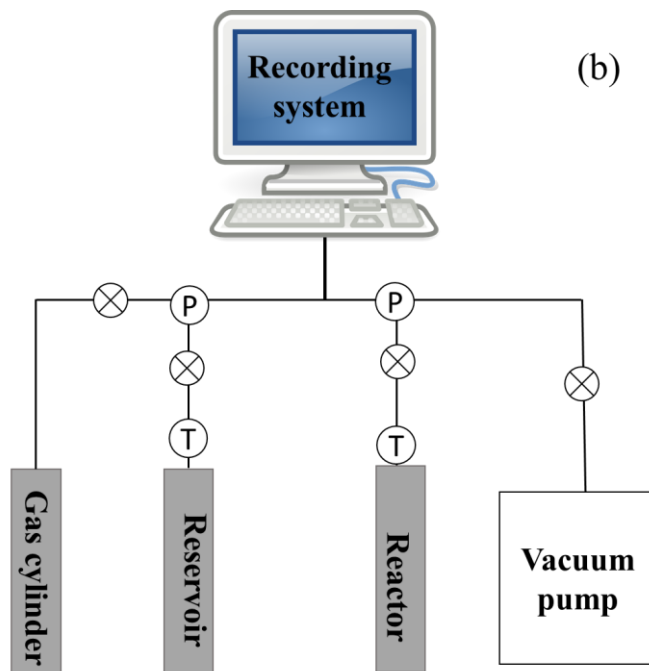


**Fig. 3.5 (a) The PCI measurement system used in this study; (b) the schematic illustration of the PCT measurement system.**

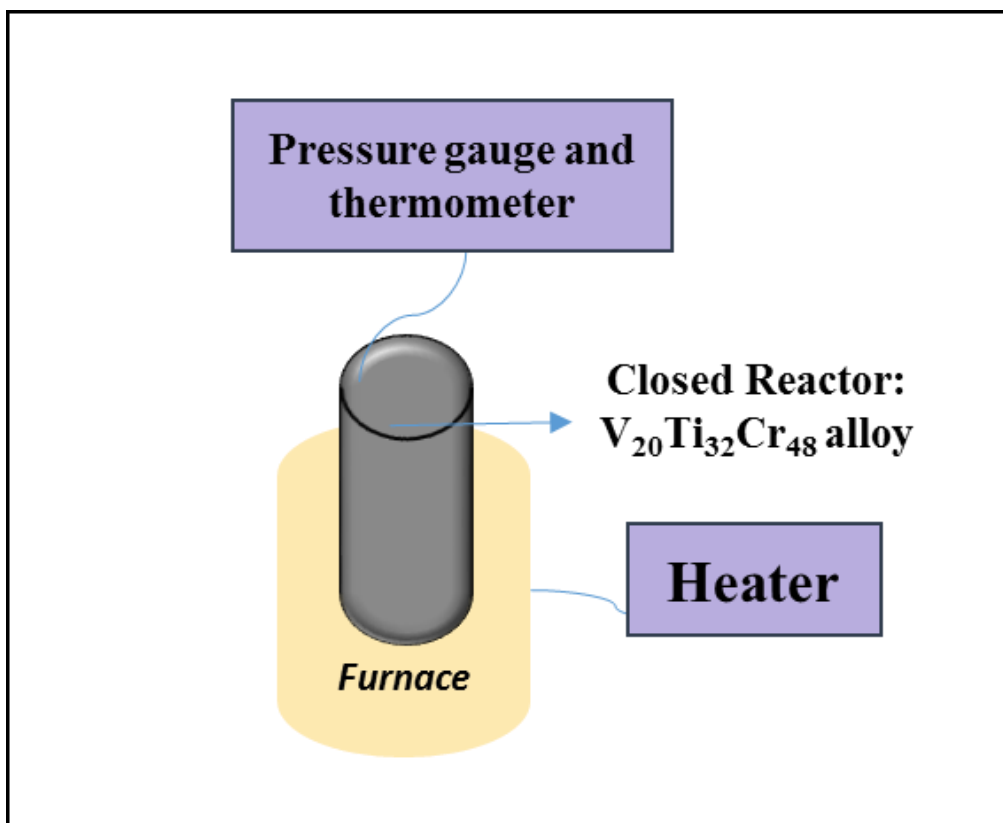


**Figure. 3.6** Homemade hydrogen compressor cycling test system.

## 4. Results and discussions

### 4.1 Hydrogen storage properties of $V_{20}Ti_{32}Cr_{48}$ at room temperature

The hydrogen storage behavior was evaluated by PCI measurements. As shown in Fig. 4.1, typical hydrogen storage behavior was observed for  $V_{20}Ti_{32}Cr_{48}$  alloy that has clear plateau pressure and can reversibly absorb 2.7 wt% hydrogen at room temperature. The plateau pressures for absorption and desorption processes were 0.4 MPa and 0.04 MPa, respectively.

In order to investigate the best conditions for the stable cyclic hydrogen compressor application without disproportionation and phase segregation, two important parameters: hydrogen content and maximum temperature were selected and individually investigated for cyclic durability of  $V_{20}Ti_{32}Cr_{48}$  alloy for hydrogen compressor test. Importantly, hydrogen content was considered as a significant factor for the first time, which could affect the cyclic durability of hydrogen compressor. Consequently, four different points were selected as starting points according to different hydrogen content on desorption curve, namely, solid solution (0%  $\beta$ -phase), half saturated (50%  $\beta$ -phase), 75% saturated (75%  $\beta$ -phase), and fully saturated (100%  $\beta$ -phase), which were shown in Fig. 4.1.

## **4.2 The influence of hydrogen content on the cyclic durability of $V_{20}Ti_{32}Cr_{48}$ alloy**

To clarify the influence of hydrogen content on the cyclic durability of  $V_{20}Ti_{32}Cr_{48}$  alloy, the max temperature of chemical hydrogen compressor was decided to fix at 260 °C, four alloy samples with different hydrogen content (solid solution, half saturated, 75% saturated, and fully saturated) were used for cycling test. For each hydrogen compressor cycling test of  $V_{20}Ti_{32}Cr_{48}$  alloy, the initial pressure of experiments was fixed in between 0.03 - 0.1 MPa at room temperature as decided by PCI desorption curve (Fig. 4.1). Then the sample cell was sealed by the valve and heated through a programmed digital thermoheater with the heating rate of 5 °C /min. After the system reached to desired temperature, the sample cell was cooled down to room temperature. This whole process was treated as 1 cycle and was repeated for 25 cycles.

### **4.2.1 $V_{20}Ti_{32}Cr_{48}$ alloy hydrogen storage behavior comparison by PCI**

Figure. 4.2 shows the PCI curves of  $V_{20}Ti_{32}Cr_{48}$  alloy at room temperature before (Fig. 4.2(a)) and after 25 compressor cycling tests that were performed with different initial hydrogen content (b - fully saturated, c - 75% saturated, d - half saturated, e - solid solution). The PCI curve of the sample just after activation shows a maximum capacity of 2.7 wt% with well-defined absorption and desorption plateau pressure at 0.4 and 0.045

MPa respectively (Fig. 4.2 (a)). After performing the hydrogen compressor cycling with the fully saturated hydrogen content alloy up to 240 °C (It is to be noted here that the temperature was stopped at 240 °C for this sample as the pressure in cell was reached to the highest limit of the cell), the hydrogen capacity was found to be decreased significantly with a sloppy plateau region as evidenced from the PCI curve shown in Fig. 4.2 (b). The behavior was quite similar in the case of cycled alloy, 75% saturated with hydrogen content. The total hydrogen storage capacity loss for both the above cases were found as 20.2% and 22.7% respectively. On the other hand, the capacity losses were found negligible for the cycled  $V_{20}Ti_{32}Cr_{48}$  alloys which contain less hydrogen initially *i.e.* 50% saturated and solid solution (Fig. 4.2 (d) and (e)). The PCI curves suggested a similar slope and stable capacity with a loss of 5.0 and 4.0 %, respectively, indicating the stable hydrogen storage capacity and good cyclic durability. Based on the above results, it can be concluded that lower initial hydrogen content in the alloy is better for hydrogen compressor cyclic durability for  $V_{20}Ti_{32}Cr_{48}$  alloy whereas the large amount of stored hydrogen in alloy leads to the reduction of reversible hydrogen storage capacity during hydrogen compression process. As a consequence, it may lead to the reduction of hydrogen compression efficiency and increasing the maintenance cost for practical usage.

#### 4.2.2 hydrogen compressor cycling test of $V_{20}Ti_{32}Cr_{48}$ alloy

As shown in Fig.4.3, for the sample with fully saturated  $H_2$ , 75% saturated  $H_2$ , half saturated  $H_2$  and solid solution, the achieved pressures at maximum temperature were: 27.8, 25.4, 14.1, and 5.1 MPa, respectively. It is obvious that the achieved hydrogen pressure was reduced with the decrease of initial hydrogen storage amount.

As shown in Fig. 4.3 (i), for the compressor test of  $V_{20}Ti_{32}Cr_{48}$  alloy with fully saturated  $H_2$  up to 240 °C, the cell pressure was increased with increasing the temperature. In the first cycle, when the aimed maximum temperature was reached to 240 °C, the pressure also reached to the maximum value of 27.8 MPa. However, this maximum pressure was gradually reduced down with number of cycles whereas the lowest pressure at room temperature was continued to increase with number of cycles. Similarly, for the compressor test of  $V_{20}Ti_{32}Cr_{48}$  alloy with 75% saturated  $H_2$  up to 260 °C, the maximum pressure was found to be changed with cycling in a similar manner as of the former one. However, the maximum achieved pressure in this case was slightly lower *i.e.* 25.4 MPa at 260 °C in first cycle, as shown in Fig.4.3 (ii). For the other cyclic data with the lower initial amount of stored hydrogen, the achieved pressure were lower and were stable during 25 cycles, as shown in Fig.4.3 (iii and iv).

To better estimate and understand the capacity degradation phenomenon, the inner

pressure at lower temperature of 32 °C was recorded and plotted versus the cycle number, because the increase in inner pressure at lower temperature must be caused by residual H<sub>2</sub> gas that could not be absorbed by the alloy in successive cycles [71]. As shown in Fig.4.4, the pressure at temperature of 32 °C was increased significantly for the cycled V<sub>20</sub>Ti<sub>32</sub>Cr<sub>48</sub> alloy with fully saturated and 75% saturated H<sub>2</sub>, which indicated that the alloy could not absorb same amount of H<sub>2</sub> gas anymore and thus, it was gradually degraded. In contrast, the pressure inside the sample holder with the V<sub>20</sub>Ti<sub>32</sub>Cr<sub>48</sub> alloy saturated with less hydrogen *i.e.* 50% and 0%, the pressure was very stable after 2<sup>nd</sup> cycle, indicating no degradation for V<sub>20</sub>Ti<sub>32</sub>Cr<sub>48</sub> alloy under these conditions.

### **4.2.3 Structure and phase characterization of V<sub>20</sub>Ti<sub>32</sub>Cr<sub>48</sub> alloy by X-ray diffraction**

To better and comprehensively understand the relationship between disproportionation phenomenon and the structure and phase changes, X-ray diffraction of cycled sample alloys were investigated. The samples were heat treated at 200 °C for 2 hours under vacuum conditions to ensure complete desorption of residual hydrogen in the samples. As shown in Fig. 4.5, the pristine V<sub>20</sub>Ti<sub>32</sub>Cr<sub>48</sub> alloy showed typical BCC structure. The cycled sample with initial lower hydrogen content (solid solution, half saturated, 75% saturated) showed similar structure as evidenced from the similar peaks

at same positions. However, all the XRD peaks were broadened a lot after hydrogen compressor cycles due to reduced crystal size caused by crystallite refinement during compressor cycles [82]. On the other side, for the cycled sample initially loaded with fully saturated H<sub>2</sub>, some multiple and overlapped peaks were appeared and new phases were confirmed as VH<sub>0.81</sub> and TiH<sub>0.66</sub> [71]. It is a direct and obvious evidence for the disproportionation due to thermodynamically favored reactions for this sample. Interestingly, according to PCI results, the sample with initial 75% saturated H<sub>2</sub> for hydrogen compressor at 260 °C also showed a large capacity loss, which was also a sign for disproportionation in a similar way. However, no big changes except broader peak width and peak intensity change were observed for this sample. Thus it is concluded that the phase separation is not the only reason for capacity fading, but the stress/strain (that can be expected from the broadening and peak intensity changes observed in XRD) generated in the material during the compressor test may also be responsible for this degradation. More supplementary technique is needed to clarify this issue.

### **4.3 Temperature influence on the cyclic durability of V<sub>20</sub>Ti<sub>32</sub>Cr<sub>48</sub> alloy**

Besides the hydrogen content influence on the cyclic durability of V<sub>20</sub>Ti<sub>32</sub>Cr<sub>48</sub> alloy, temperature impact should also not be negligible. Thus in this work, the investigation of

the temperature influence on the cyclic durability for  $V_{20}Ti_{32}Cr_{48}$  alloy employed for compressor was also conducted. To do this, the hydrogen content of initial state was fixed as three groups: fully saturated, half saturated and solid solution. The maximum temperatures were chosen as 260, 200, 175, 150, and 100 °C for each initial hydrogen capacity according to desorption PCI curve as mentioned earlier.

#### **4.3.1 Hydrogen compressor cycling test of $V_{20}Ti_{32}Cr_{48}$ alloy with fully saturated $H_2$ up to different temperatures**

As shown in Fig. 4.6, the achieved pressure for the sample with fully saturated  $H_2$  after reaching to different maximum temperature were: 27.8, 14.9, 11.0, 5.7, and 2.1 MPa, respectively. It is obvious that the achieved maximum hydrogen pressure was reduced with lowering the maximum temperature.

Similarly, the inner pressure at lower temperature of 32.3 °C at the end of each cycle was also recorded to evaluate the hydrogen compressor cycling behavior. As shown in Fig. 4.7 the pressure was increased with the number of cycles for the  $V_{20}Ti_{32}Cr_{48}$  alloy cycled up to 240 and 200 °C, which indicated the gradual degradation of the alloy. In contrast, the  $V_{20}Ti_{32}Cr_{48}$  alloy cycled up to 175, 150, and 100 °C temperatures, the pressure was very stable after 2<sup>nd</sup> cycle, indicating the stable cyclic durability during 25 cycles.

### **4.3.2 Temperature influence on the cyclic durability of $V_{20}Ti_{32}Cr_{48}$ alloy with fully saturated $H_2$ content**

The PCI curves of  $V_{20}Ti_{32}Cr_{48}$  alloy with fully saturated  $H_2$  after 25 hydrogen compressor cycles up to 240 °C (Fig. 4.8 (b)) clearly showed worst performance with significant hydrogen storage capacity loss (20.2% of initial capacity) and increased slope, which indicated a significant reduction in reversible capacity. For the  $V_{20}Ti_{32}Cr_{48}$  alloy cycled for hydrogen compressor up to 200 °C (Fig. 4.8(c)), the hydrogen storage capacity loss after 25 cycles was 17.9% of initial capacity, which was little less than the  $V_{20}Ti_{32}Cr_{48}$  alloy cycled at 240 °C. Moreover, the slope of the PCI curves of this sample was also not changed as much as the former one. In both cases, the capacity loss was huge enough and could be treated as a result of disproportionation. On the other hand,  $V_{20}Ti_{32}Cr_{48}$  alloy cycled up to 175, 150, and 100 °C showed comparatively less capacity losses around 4 to 5% with similar PCI slope and stable hydrogen storage capacity, indicating the good cyclic durability under these conditions. Based on above results, it can be concluded that lower temperature is better for the compressor cyclic durability of  $V_{20}Ti_{32}Cr_{48}$  alloy whereas, higher temperature lead the degradation of this alloy and reduce the hydrogen storage capacity followed by the decrease of hydrogen compression ratio during practical usage.

### **4.3.3 Temperature influence on the cyclic durability of $V_{20}Ti_{32}Cr_{48}$ alloy with half saturated $H_2$ content**

The PCI curves of  $V_{20}Ti_{32}Cr_{48}$  alloy with half saturated  $H_2$  at RT before and after 25 hydrogen compressor cycling tests up to different temperature showed quite different behavior in comparison to that for fully saturated case. As shown in Fig. 4.9, the room temperature PCI isotherm curves of half saturated  $V_{20}Ti_{32}Cr_{48}$  alloy before and after 25 hydrogen compression cycling tests up to different maximum temperature showed similar slope and almost similar capacity losses: 4.13% at 260 °C, 3.55% at 200 °C, 5.92% at 150 °C and 4.57% at 100 °C, respectively. It demonstrated that the alloy was stable under these conditions and could be used for further.

Compared with the fully saturated cases, the achieved maximum hydrogen pressure of the  $V_{20}Ti_{32}Cr_{48}$  alloy with half saturated  $H_2$  is slightly lower, which are 14.1 MPa at 260 °C, 13.4 MPa at 200 °C, 5.4 MPa at 150 °C and 1.1 MPa at 100 °C, respectively (shown in Fig. 4.10). The achieved maximum pressure during 25 compressor tests are concordant with the initial cycle. The great stability and durability can be expected if we utilize this alloy with half saturated  $H_2$  for hydrogen compressor application.

The inner pressure at lower temperature of 32.3 °C at the end of each cycle was also plotted to evaluate the hydrogen compressor cycling behavior. As shown in Fig.4.11,

differing from the former cases, the inner pressure was slightly increased after 2<sup>nd</sup> cycles, and remained stable during all the cycles, indicating the stable releasing amount of hydrogen and hydrogen pressure during 25 cycles.

#### **4.3.4 Temperature influence on the cyclic durability of V<sub>20</sub>Ti<sub>32</sub>Cr<sub>48</sub> alloy with solid solution of hydrogen**

Similar to half saturated cases, the PCI curves of V<sub>20</sub>Ti<sub>32</sub>Cr<sub>48</sub> alloy with solid solution at RT before and after 25 hydrogen compressor cycling tests up to different temperatures acted in the same way. As shown in Fig. 4.12, the room temperature PCI isotherm curves of V<sub>20</sub>Ti<sub>32</sub>Cr<sub>48</sub> alloy with solid solution before and after 25 hydrogen compression cycling tests up to different maximum temperature showed similar slope and similar capacity losses: 5.10% at 260 °C, 4.45% at 200 °C, 1.30% at 150 °C and 4.24% at 100 °C, respectively. It suggested that the alloy was stable enough and had a good cyclic durability and could be potentially used for further.

Fig.4.13 shows the pressure and temperature changes during 25 cyclic compressor tests of V<sub>20</sub>Ti<sub>32</sub>Cr<sub>48</sub> alloy with solid solution up to (i) 260 °C; (ii) 200 °C; (iii) 150 °C and (iv) 100 °C. If we compare it with Fig.4.6 and 4.10, it is easy to find that the achieved maximum hydrogen pressure of the V<sub>20</sub>Ti<sub>32</sub>Cr<sub>48</sub> alloy with solid solution is lowest in three groups because of the lowest initial hydrogen absorption amount in alloy matrix, which

are 5.1 MPa at 260 °C, 7.8 MPa at 200 °C, 1.3 MPa at 150 °C, and 1 MPa at 100 °C, respectively. The achieved maximum pressures during 25 compressor tests are constant during 25 compressor cycles. In this way, it is possible to use this alloy at higher temperature with considerable achieved compression H<sub>2</sub> pressure for long term application without disproportion and efficiency loss.

Correspondingly, the inner pressure at lower temperature of 32.3 °C at the end of each cycle was also recorded to evaluate the hydrogen compressor cycling behavior. As shown in Fig.4.14, the inner pressure has the same variation as that of the half saturated case, which was also slightly increased after 2<sup>nd</sup> cycles, and remained stable during 25 cycles. This indicated the stable cyclic durability during 25 cycles' compression.

#### **4.3.5 Structure and phase characterization of V<sub>20</sub>Ti<sub>32</sub>Cr<sub>48</sub> alloy with different hydrogen content under temperature influence by X-ray diffraction**

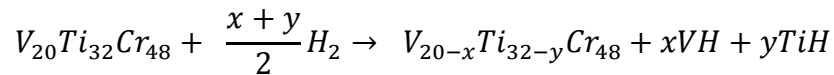
The structural and phase changes under different conditions as mentioned in 4.3.1 – 4.3.4, were also investigated by X-ray diffraction. As shown in Fig. 4.15, Fig. 4.16, and Fig. 4.17, the pristine V<sub>20</sub>Ti<sub>32</sub>Cr<sub>48</sub> alloy showed typical BCC structure. All the samples except the cycled sample with initial fully saturated H<sub>2</sub> content up to 240 °C, showed similar structure as evidenced from the presence of peaks at same position. However, the

XRD peaks were broadened after hydrogen compressor cycles due to reduced crystallite size caused by pulverization. What's more, the intensity of the peak at  $61.02^\circ$  was decreased, which might probably be caused by the structure changes from BCC to BCT structure when formed some V hydrides phase. On the other hand, the fully saturated sample cycled at  $240^\circ\text{C}$  showed some multiple and overlapped peaks which could be indexed by  $\text{VH}_{0.81}$  and  $\text{TiH}_{0.66}$  phases [71]. It is a direct and obvious evidence for the disproportionation, occurred at this temperature. Interestingly, according to PCI results, the sample for hydrogen compressor at  $200^\circ\text{C}$  also showed large capacity loss, which was a sign of disproportionation. However, no big changes or new phase formation could be observed from XRD results. Thus the large capacity loss could not be explained only on the basis of structural changes, but other factors like stress/strain generation also play an important role for this capacity loss [81].

#### **4.4 Structural and morphology investigation of pristine and disproportionated $\text{V}_{20}\text{Ti}_{32}\text{Cr}_{48}$ alloys by SEM and EDS mapping technique**

Figure 4.18 shows SEM morphology of pristine and cycled (up to  $240^\circ\text{C}$ ) samples of  $\text{V}_{20}\text{Ti}_{32}\text{Cr}_{48}$  with fully saturated  $\text{H}_2$ . The size of pristine sample was not so uniform and in the range of several micrometers to hundred micrometers. After cycling, the average

size of the sample was found to be reduced along with several cracks, which must be caused by pulverization during extended hydrogenation and dehydrogenation cycling processes. Moreover, point analysis was conducted by EDS to check the content of each components in  $V_{20}Ti_{32}Cr_{48}$  alloys. Table. 4.1 shows the atomic percentage of elements in  $V_{20}Ti_{32}Cr_{48}$  alloy as determined by EDS analysis. The point no. corresponds to the different positions as shown in Fig.4.18 (b) and (d). The atomic percentage of V, Ti, Cr elements in pristine  $V_{20}Ti_{32}Cr_{48}$  alloy as determined by EDS analysis were very similar to the actual composition *i.e.* 20, 32, 48, respectively. However, after cycling, some Ti-rich phase was found as shown in Fig. 4.18 (d). On the basis of XRD and SEM-EDS results, a possible hypothetical qualitative reaction corresponding to the disproportionation of  $V_{20}Ti_{32}Cr_{48}$  alloy can be proposed as:



According to the above EDS results, the Ti atomic percentage at special point was increased up to more than 60, followed by the reduction of V and Cr atomic percentage. This clearly shows the disproportionation of  $V_{20}Ti_{32}Cr_{48}$  alloy with fully saturated  $H_2$ , cycled up to 240 °C.

## 4.5 Summary of hydrogen compressor test of $V_{20}Ti_{32}Cr_{48}$ alloy.

Various achieved temperature and hydrogen content conditions were controlled for hydrogen compressor cycling tests of  $V_{20}Ti_{32}Cr_{48}$  alloy. Table. 4.2 shows the summary of all the information, such as pressure, capacity, and temperature.

These results are plotted in the following Fig. 4.19 (a, b, and c). The achieved maximum pressure and temperature were plotted in Fig. 4.19(a). As we can see, the achieved maximum pressure is increased with the increase in temperature, which is quite reasonable according to Van der Waal's equation. Hydrogen content and temperature influence was checked by plotting the capacity loss (in percentage, from the PCI curves before and after 25 hydrogen compressor cycles) with these two parameters. Since the amount of hydrogen left in the alloy at maximum temperature plays an important role in the disproportionation process, so it was calculated according to pressure, temperature, alloy amount, and sample cell volume. For example, the pristine  $V_{20}Ti_{32}Cr_{48}$  alloy of 16.65g was filled with hydrogen gas to fully saturated state. The starting temperature for  $H_2$  filling was 23.2 °C, the pressure was 0.074 MPa. The reactor volume was 19.23 cm<sup>3</sup> and the hydrogen amount in the alloy was 2.43wt%. The total amount of hydrogen in the sealed sample cell  $H_{Total}$  consisted of two parts as shown in Fig 4.20: hydrogen in the

metal  $H_M$  and hydrogen in the upper gas phase  $H_{gas}$ .

$$H_{Total} = H_M + H_{gas}$$

$$H_M = M \times 2.43\text{wt}\% = 16.65\text{g} \times 2.43\text{wt}\% = 0.41\text{g}$$

To calculate the hydrogen amount in the gas phase, the density of  $H_2$  should be known. According to NIST Chemistry WebBook [84], the density of  $H_2$  gas  $\rho$  can be easily obtained by inputting the actual temperature and pressure. For the  $H_2$  gas at 23.2 °C with pressure of 0.074 MPa, the density is  $6.05 \times 10^{-5} \text{ g/cm}^3$ .

$$H_{gas} = \rho \times V_{gas} = \rho \times (V_{total} - V_M) = 6.05 \times 10^{-5} \text{ g/cm}^3 \times (19.23 - 16.65\text{g}/6\text{g/cm}^3) = 0.00099\text{g}$$

$$\text{So, } H_{Total} = H_M + H_{gas} = 0.40\text{g} + 0.00099\text{g} = 0.41 \text{ g}$$

Similar calculation can be done when the sample was heated to higher temperature 240 °C, the achieved pressure was 27.8 MPa and the density of hydrogen in the gas phase at this state was  $0.012 \text{ g/cm}^3$ .

$$H_{gas} = \rho \times V_{gas} = \rho \times (V_{total} - V_M) = 0.012 \text{ g/cm}^3 \times (19.23 - 16.65\text{g}/6\text{g/cm}^3) = 0.20 \text{ g}$$

$$H_M = H_{Total} - H_{gas} = 0.41 \text{ g} - 0.20 \text{ g} = 0.21\text{g}$$

So the hydrogen amount in the alloy is:

$$0.21\text{g}/16.65\text{g} \times 100 = 1.2 \text{ wt}\%.$$

Where,  $M$  is the weight of alloy sample,  $V_{total}$  is the volume of sample cell.  $V_{gas}$  is

the volume that hydrogen gas occupied and  $V_M$  represents the volume that alloy sample occupied.

Same calculations were conducted for other cases, all the details and results were summarized in Table. 4.2.

In order to understand the hydrogen content influence, Fig. 4.19(b) was plotted. It can be clearly seen that, the  $V_{20}Ti_{32}Cr_{48}$  alloy saturated with  $H_2$  more than 75%, lost significant hydrogen storage capacity (~20%), while for other cases, the capacity loss is quite small (< 8%). Thus, there is an obvious boundary between the conditions for disproportionation and stability.

The temperature effect on the compressor cycling test is shown in Fig. 4.19(c).  $V_{20}Ti_{32}Cr_{48}$  alloys saturated with more than 75%  $H_2$  was disproportionated at temperature higher than 200 °C, which can be considered as boundary temperature for the disproportionation. To define a boundary line for disproportionation, the hydrogen content remained in the alloy is plotted against the maximum temperature as shown in Fig. 4.19(d). At the same temperature, the sample that holds more hydrogen at initial stage before compressor cycle test, contains more hydrogen in solid phase after reaching achieved temperature. In order to get a boundary, the black solid line was drawn based on the experimental disproportionation data by combining all the above results including

XRD. A dashed horizontal line was drawn in order to show the maximum hydrogen content that can be held by alloy. It is important to note here that all the BCC alloys in general can withstand with very high temperature in the absence of hydrogen in it. Thus the disproportionation that is observed here, must be caused by the solid hydrogen present in the alloy. It is also noted here that the slope line become horizontal around the remaining hydrogen content of 2.1 wt% due to the experimental limitations as we could not perform experiment at more extreme condition. If we assume that more hydrogen can be remained in the alloy by applying more extreme conditions, it may cause a disproportionation even at low temperature. However, it can be obtained, if the slope line (blue colored) is extended vertically upwards as shown in the Fig. 4.19(d). Thus, the area covered by horizontal and slope line through their cross (gray colored area in Fig. 4.19(d)) can be a guide for the suitable operating condition for this alloy. The area left of the blue colored line is suitable for this alloy, whereas all the rest conditions will give rise a disproportionation of this alloy during cycling.

## Figures

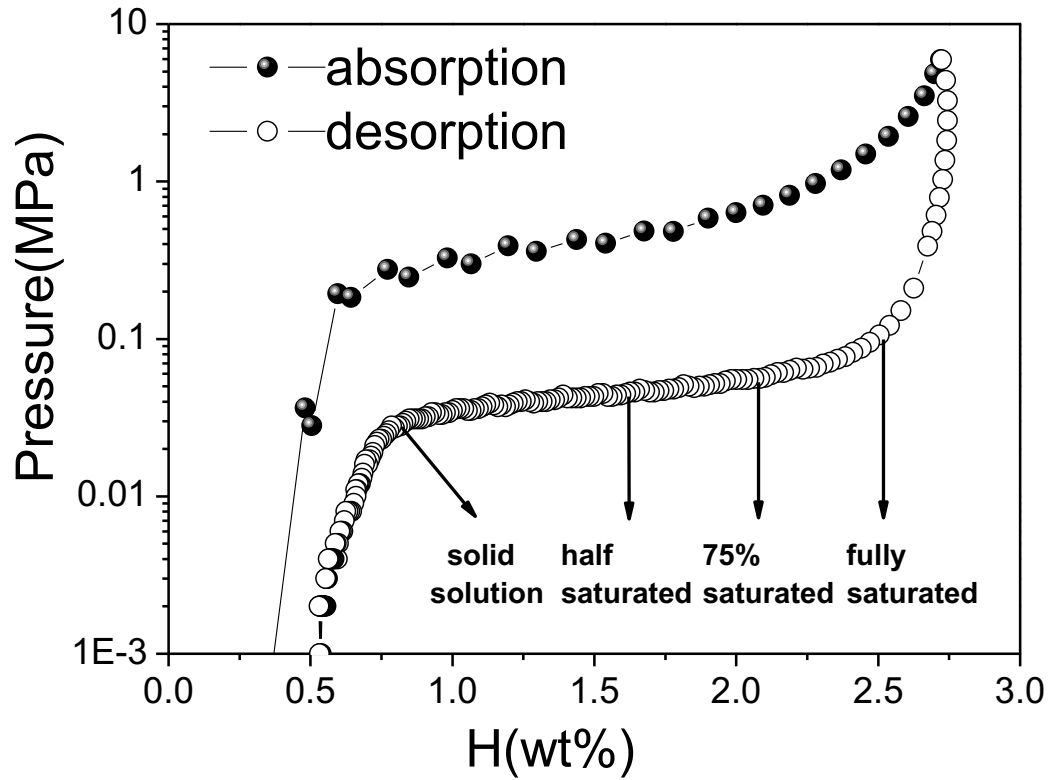
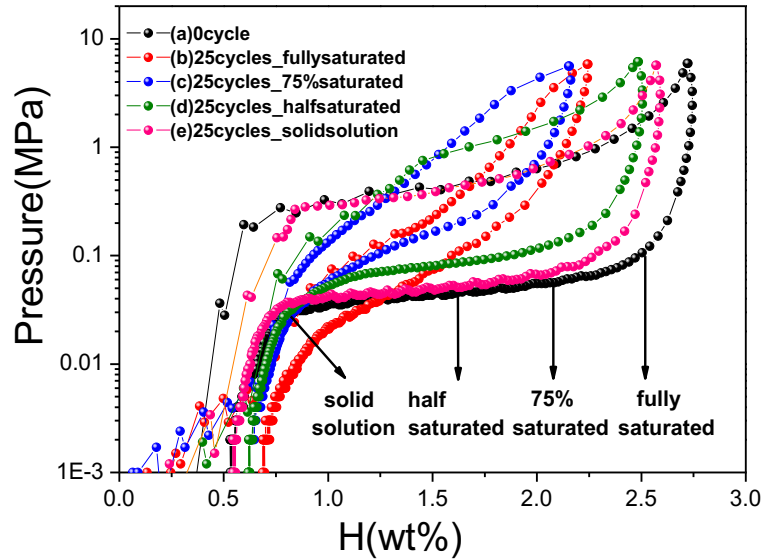
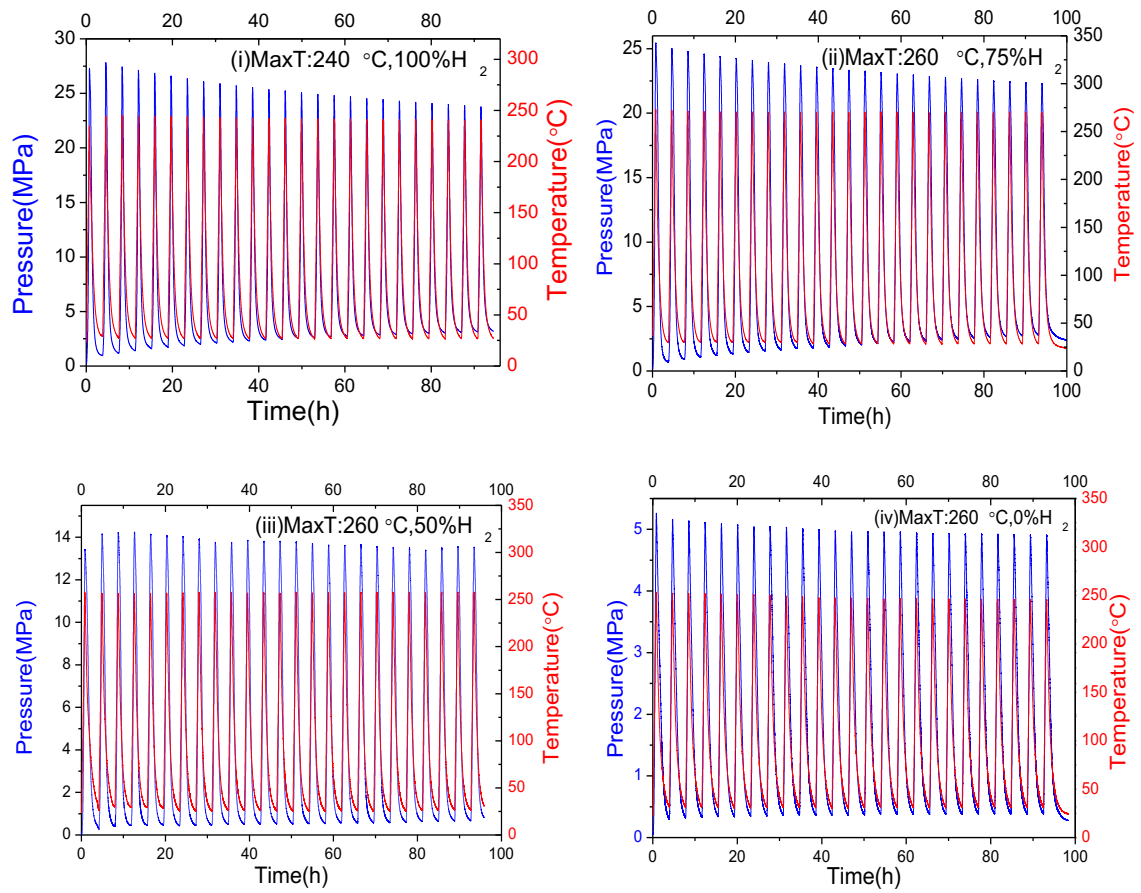


Figure 4.1 PCI curve of  $V_{20}Ti_{32}Cr_{48}$  alloy at room temperature.



**Figure 4.2 Room temperature PCI curves of  $V_{20}Ti_{32}Cr_{48}$  alloy (a) before and (b-e) after 25 hydrogen compressor cycling tests up to high temperature (b: up to 240 °C and c, d and e: up to 260 °C). The starting point was decided according to different hydrogen content: b) solid solution, c) half saturated, d) 75% saturated, e) fully saturated.**



**Figure 4.3 (i) Pressure and temperature changes during 25 cyclic compressor tests of  $V_{20}Ti_{32}Cr_{48}$  alloy with fully saturated  $H_2$  up to 240 °C; (ii) 75 % saturated  $H_2$  up to 260 °C; (iii) 50% saturated  $H_2$  up to 260 °C and (iv) 0% saturated  $H_2$  up to 260 °C.**

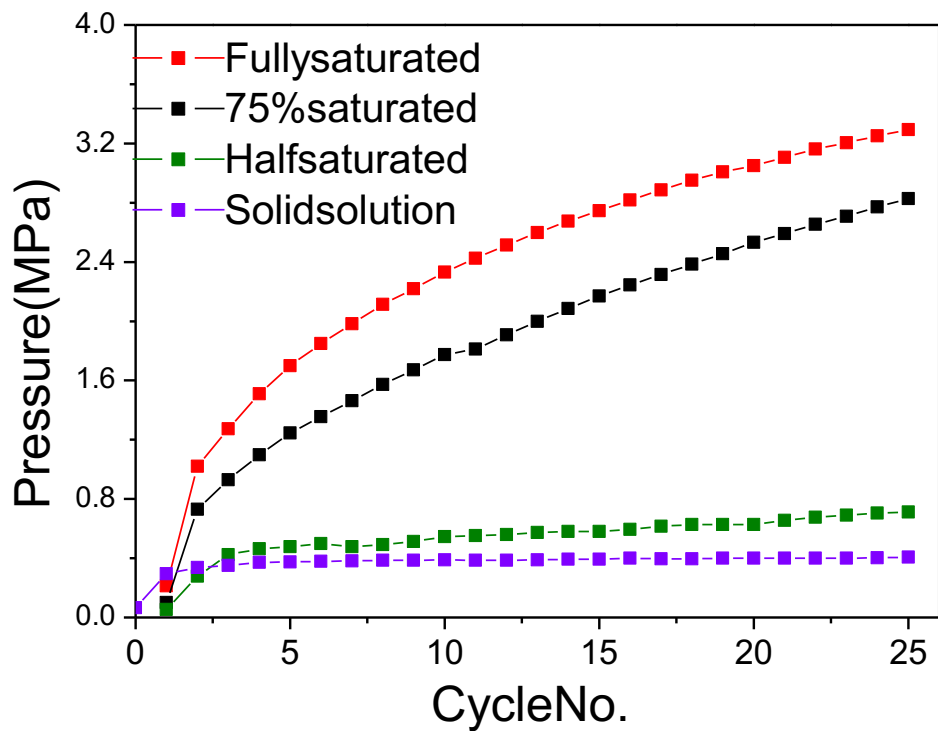


**Figure 4.4 Cyclic compressor performance comparison of  $V_{20}Ti_{32}Cr_{48}$  alloy with different initial hydrogen content in terms of system pressure variation at low temperature of 32.3 °C with no. of cycles.**

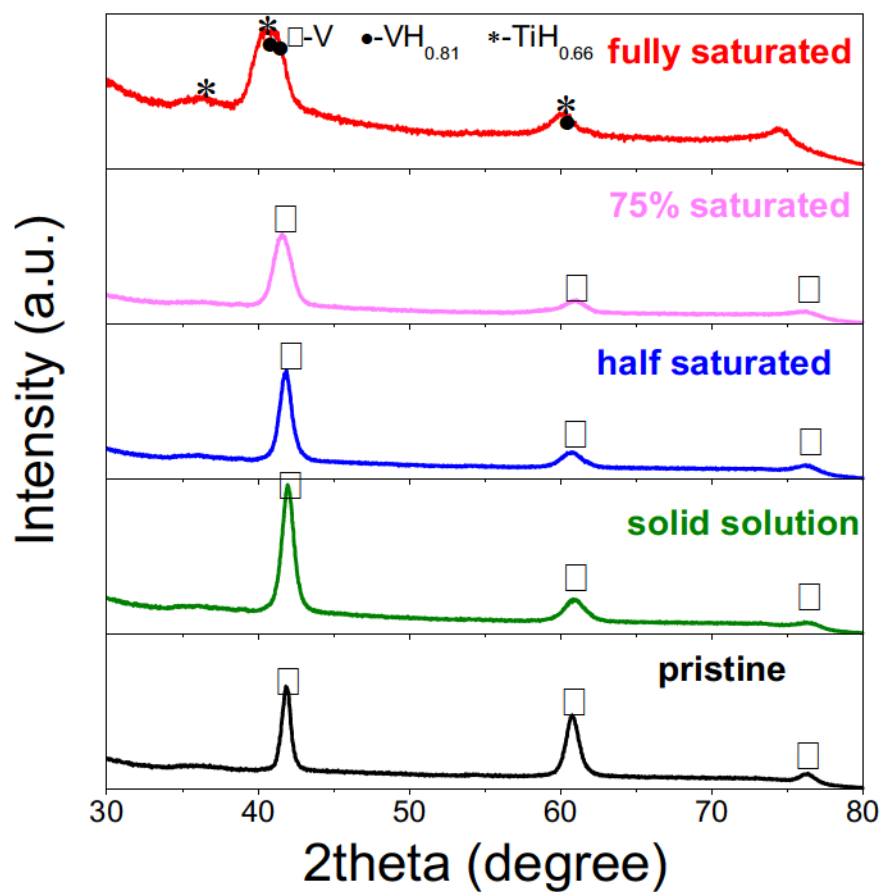


**Figure 4.5 XRD profiles of  $V_{20}Ti_{32}Cr_{48}$  alloy before and after compressor cycling with different initial hydrogen content.**

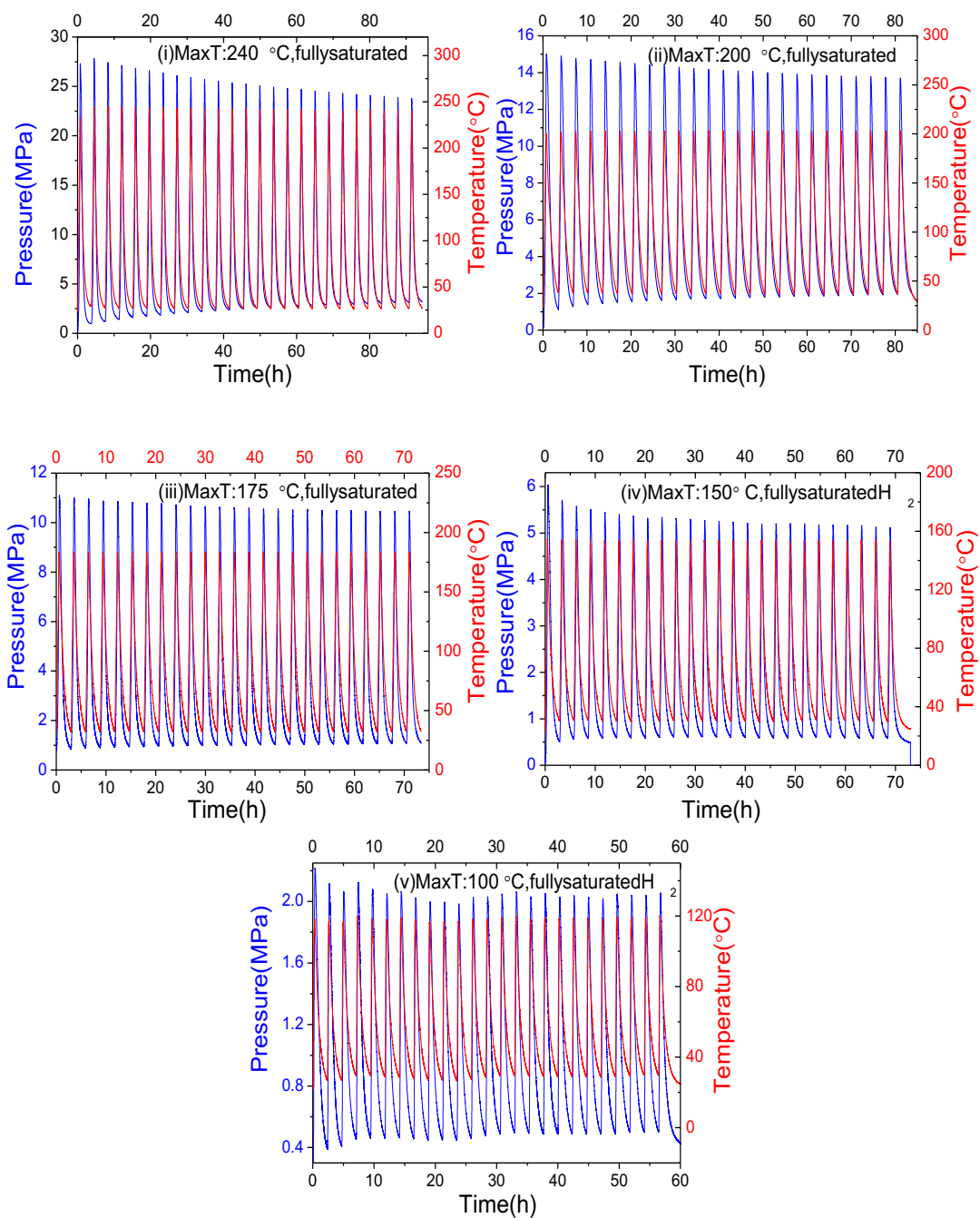


**Figure 4.6 Pressure and temperature changes during 25 cyclic compressor tests of  $V_{20}Ti_{32}Cr_{48}$  alloy with fully saturated  $H_2$  up to (i) 240 °C; (ii) 200 °C; (iii) 175 °C; (iv) 150 °C and (v) 100 °C.**

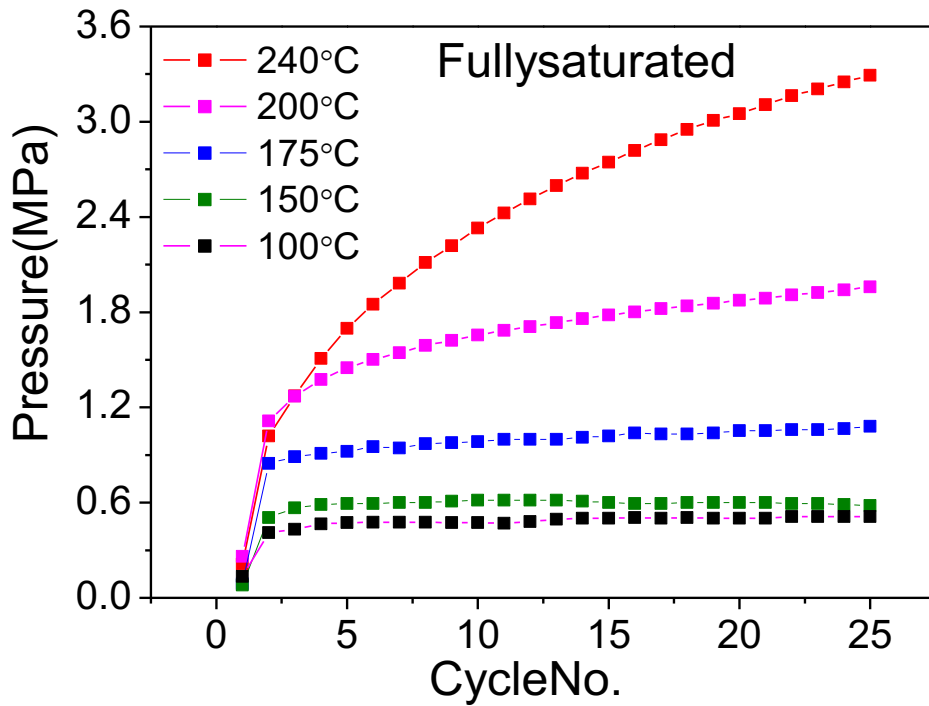


**Figure 4.7 Cyclic compressor performance comparison of  $V_{20}Ti_{32}Cr_{48}$  alloy with fully saturated  $H_2$  hydrogen content at different temperature in terms of system pressure variation at low temperature of  $32.3\text{ }^\circ\text{C}$  with no. of cycles.**

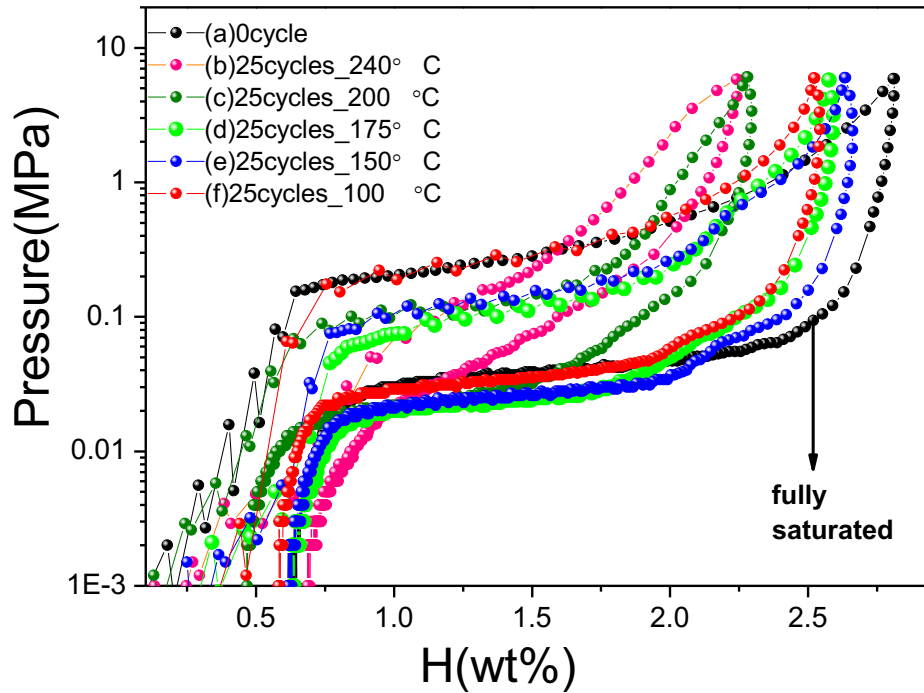


**Figure 4.8 PCI curves of  $V_{20}Ti_{32}Cr_{48}$  alloy with fully saturated  $H_2$  at RT: (a) before; and after 25 hydrogen compressor cycling tests up to high temperatures - (b) up to 240 °C; (c) up to 200 °C; (d) up to 175 °C; (e) up to 150 °C and (f) up to 100 °C. The starting point was decided according to same hydrogen content: fully saturated.**

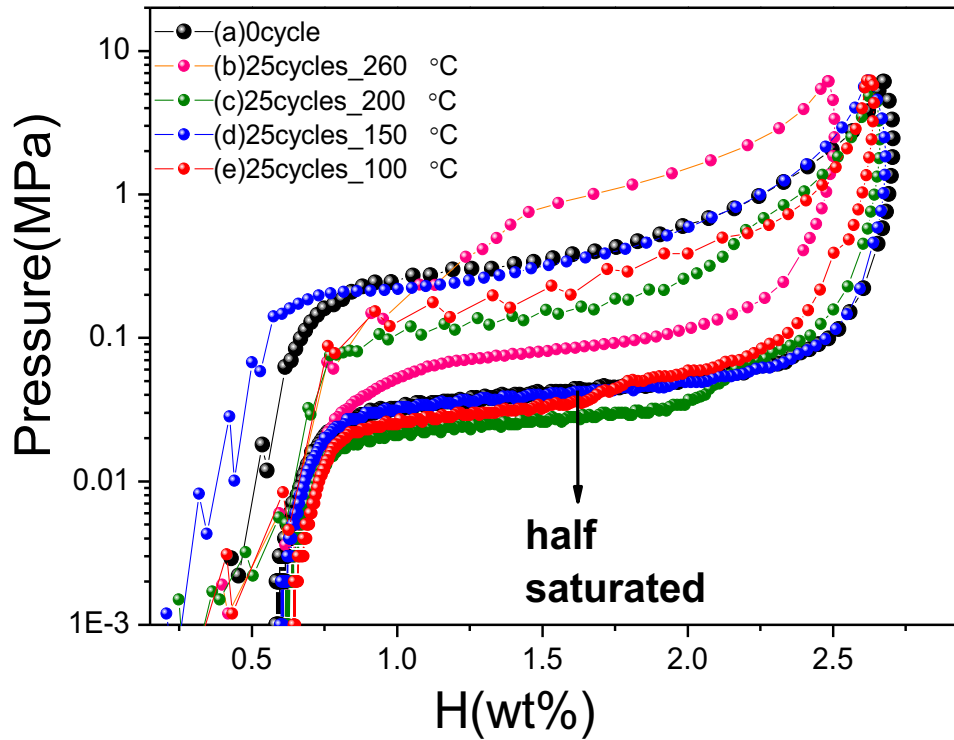


**Figure 4.9 PCI curves of V<sub>20</sub>Ti<sub>32</sub>Cr<sub>48</sub> alloy with half saturated H<sub>2</sub> at RT: (a) before; and after 25 hydrogen compressor cycling tests up to high temperatures - (b) up to 260 °C; (c) up to 200 °C; (d) up to 150 °C and (e) up to 100 °C. The starting point was decided according to same hydrogen content: half saturated.**

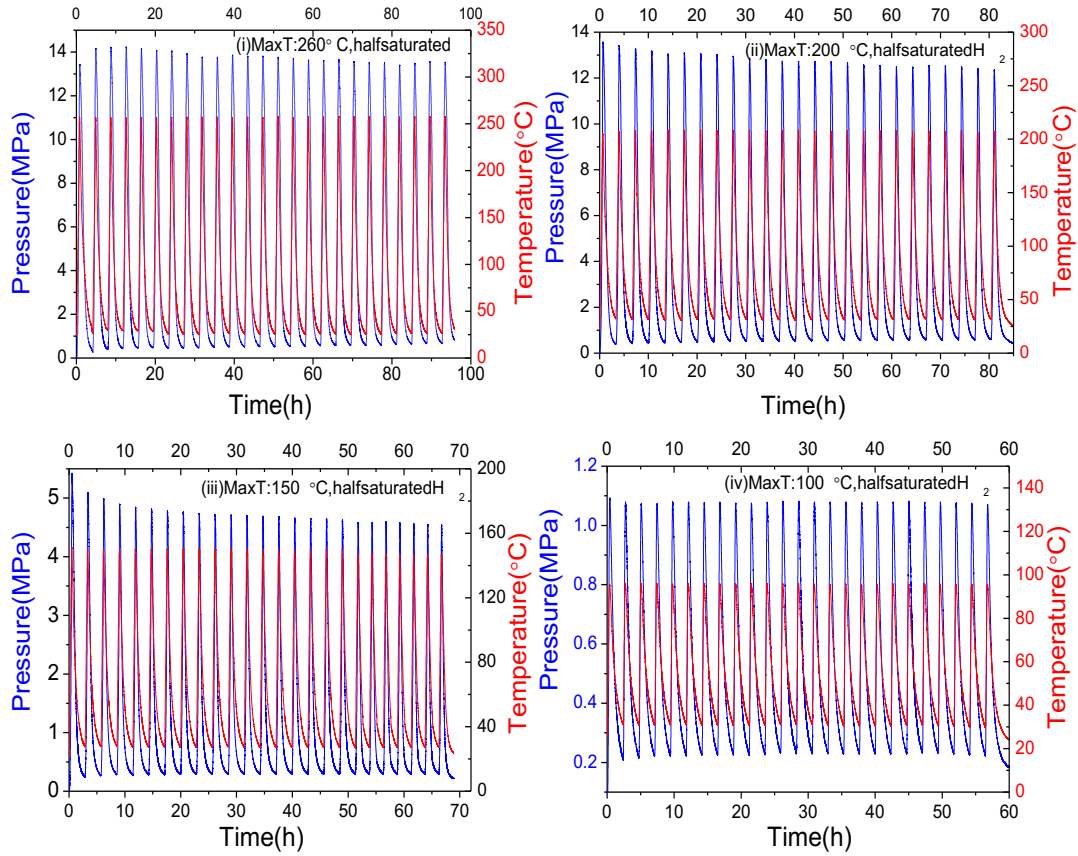


**Figure 4.10 Pressure and temperature changes during 25 cyclic compressor tests of  $V_{20}Ti_{32}Cr_{48}$  alloy with half saturated  $H_2$  up to (i) 260 °C; (ii) 200 °C; (iii) 150 °C and (iv)100 °C.**

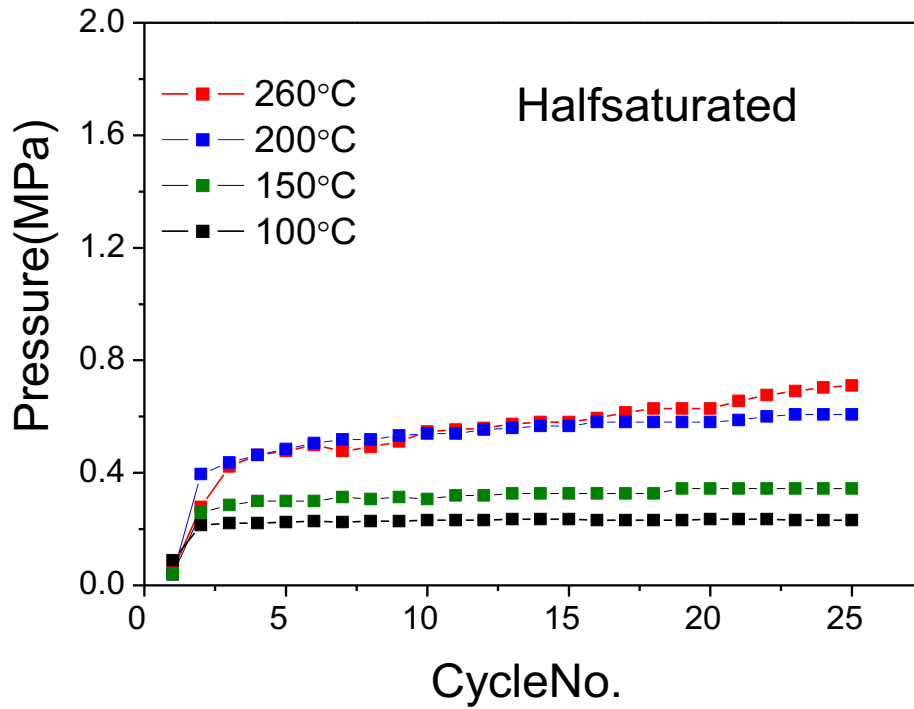


**Figure 4.11 Cyclic compressor performance comparison of  $V_{20}Ti_{32}Cr_{48}$  alloy with half saturated  $H_2$  hydrogen content at different temperature in terms of system pressure variation at low temperature of  $32.3\text{ }^\circ\text{C}$  with no. of cycles.**

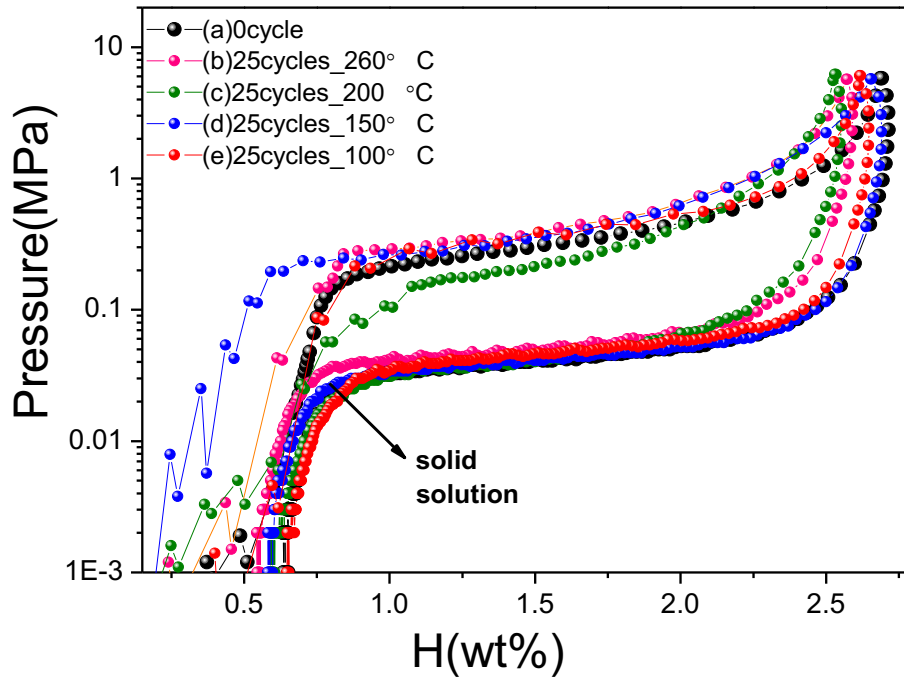


**Figure 4.12** PCI curves of V<sub>20</sub>Ti<sub>32</sub>Cr<sub>48</sub> alloy with 0% saturated H<sub>2</sub> (solid solution) at RT: (a) before; and after 25 hydrogen compressor cycling tests up to high temperatures - (b) up to 260 °C; (c) up to 200 °C; (d) up to 150 °C and (e) up to 100 °C. The starting point was decided according to same hydrogen content: solid solution.

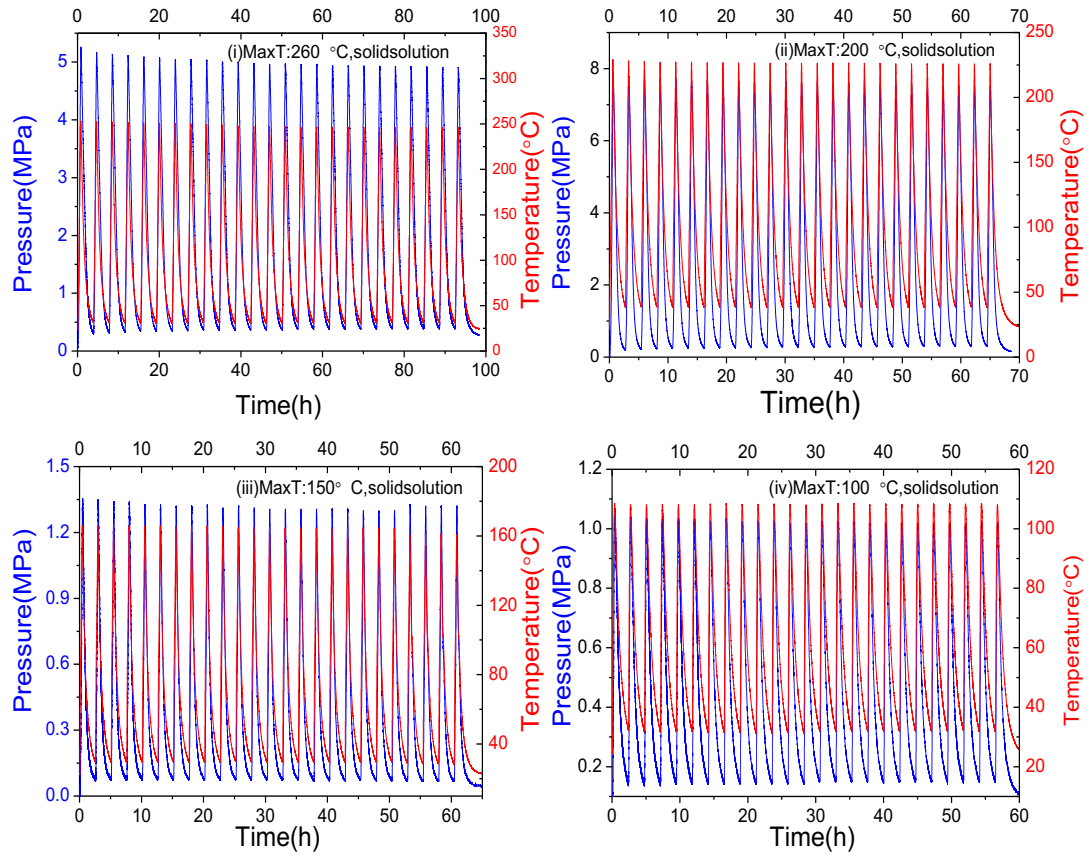


**Figure 4.13 Pressure and temperature changes during 25 cyclic compressor tests of  $V_{20}Ti_{32}Cr_{48}$  alloy with solid solution up to (i) 260  $^{\circ}C$ ; (ii) 200  $^{\circ}C$ ; (iii) 150  $^{\circ}C$  and (iv) 100  $^{\circ}C$ .**

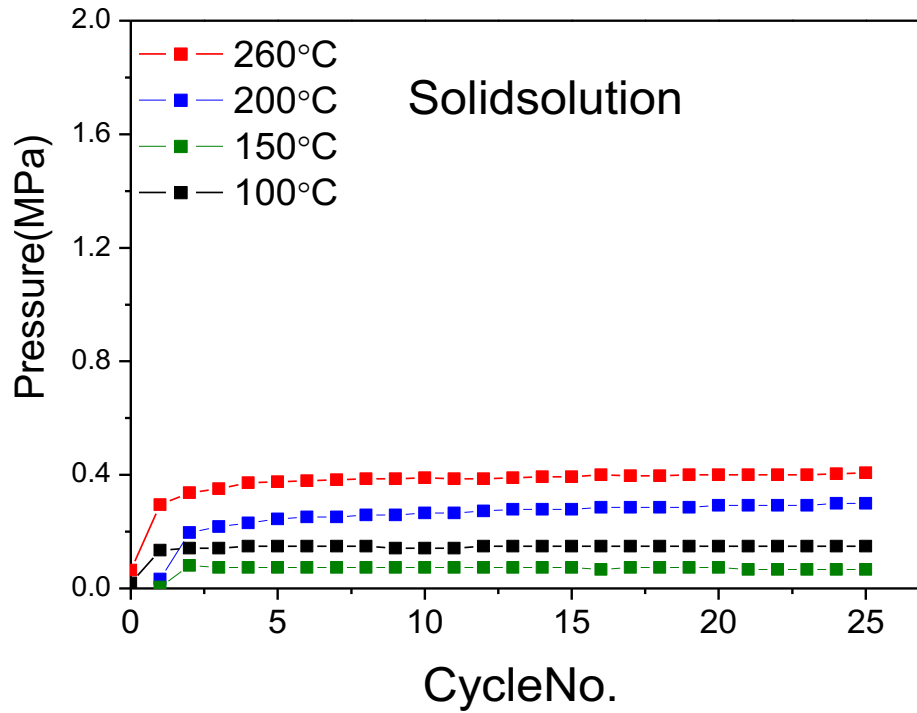


**Figure 4.14 Cyclic compressor performance of  $V_{20}Ti_{32}Cr_{48}$  alloy with solid solution in terms of system pressure variation at low temperature of  $32.3\text{ }^{\circ}C$  with no. of cycles.**

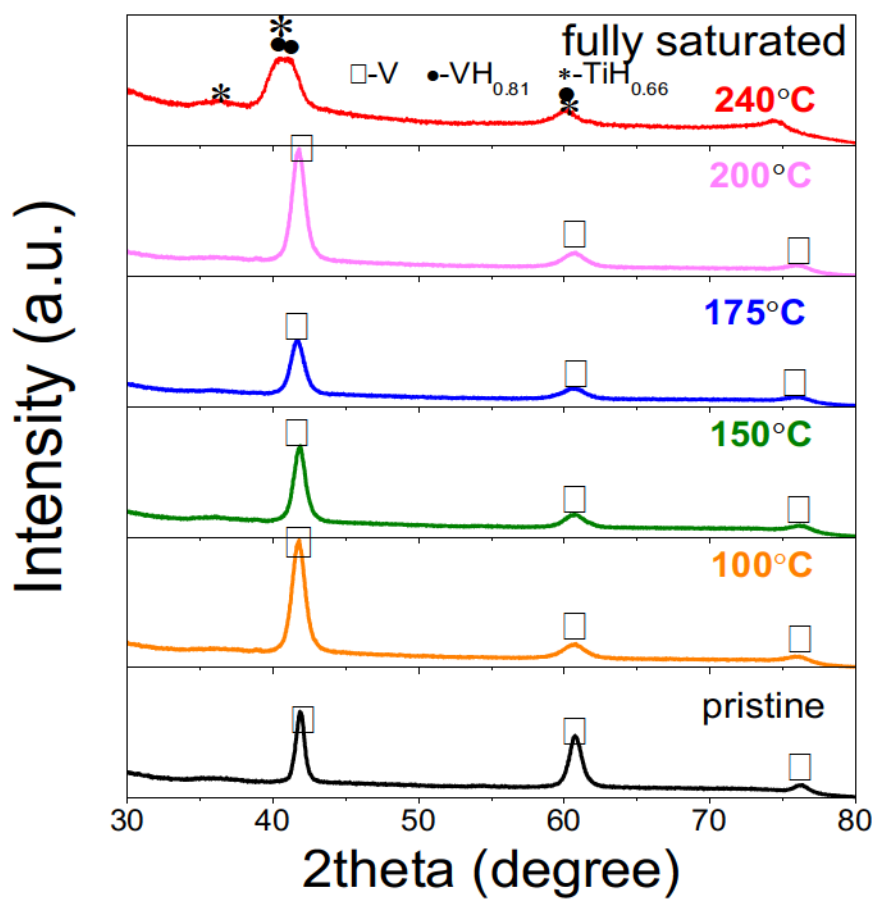


**Figure 4.15 XRD of  $V_{20}Ti_{32}Cr_{48}$  alloy with fully saturated  $H_2$  after 25 hydrogen compressor cycles up to 100 °C, 150 °C, 175 °C, 200 °C and 240 °C.**

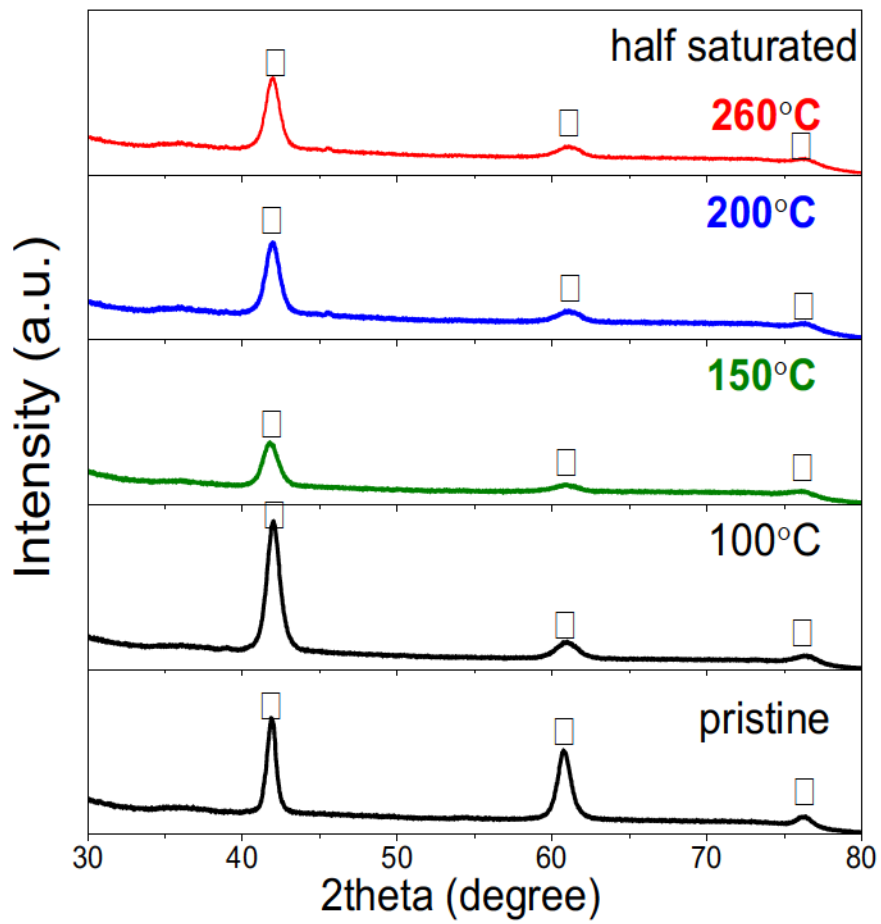


**Figure 4.16** XRD of  $V_{20}Ti_{32}Cr_{48}$  alloy with half saturated  $H_2$  after 25 hydrogen compressor cycles up to 100 °C, 150 °C, 200 °C and 260 °C.

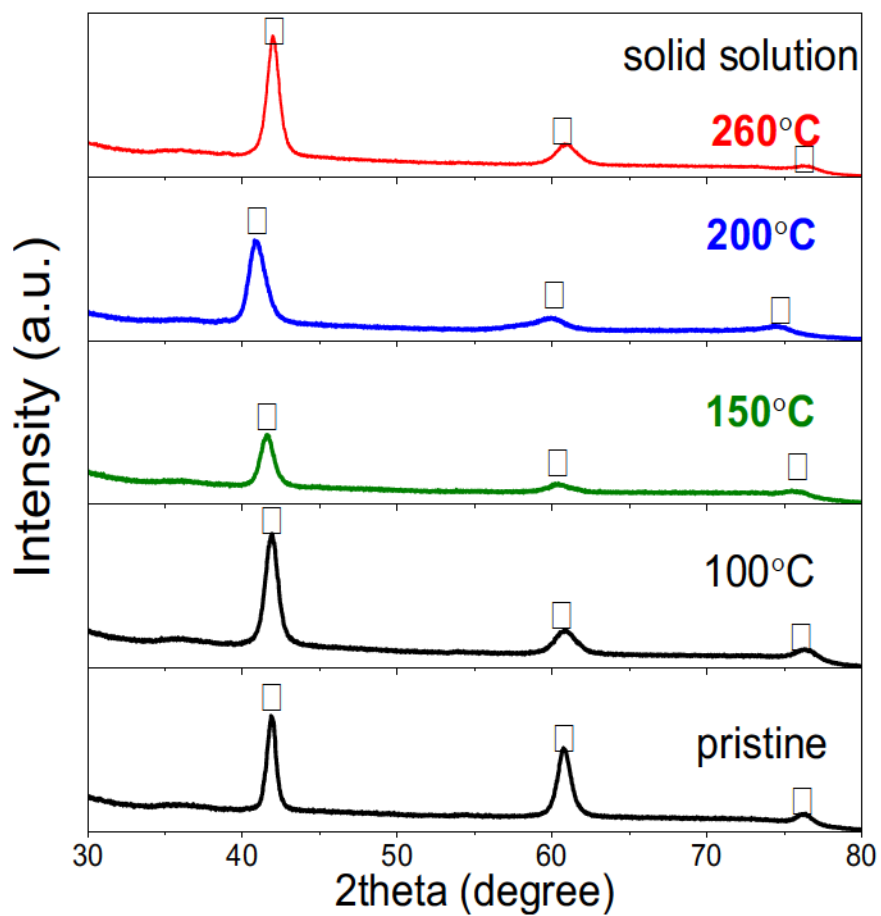


**Figure 4.17 XRD of  $V_{20}Ti_{32}Cr_{48}$  alloy with solid solution after 25 hydrogen compressor cycles up to  $100^{\circ}C$ ,  $150^{\circ}C$ ,  $200^{\circ}C$  and  $260^{\circ}C$ .**

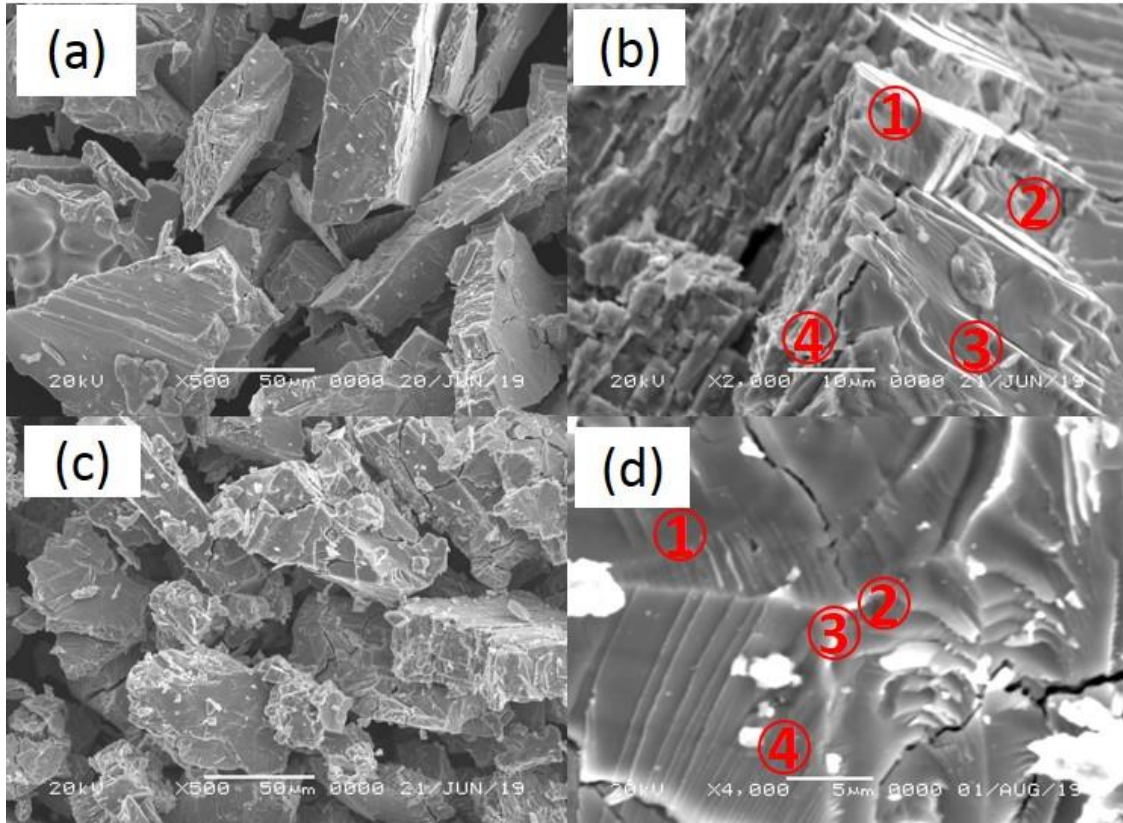


**Figure 4.18 SEM morphology of pristine (a and b) and cycled (c and d) sample up to 240 °C with fully saturated H<sub>2</sub>.**

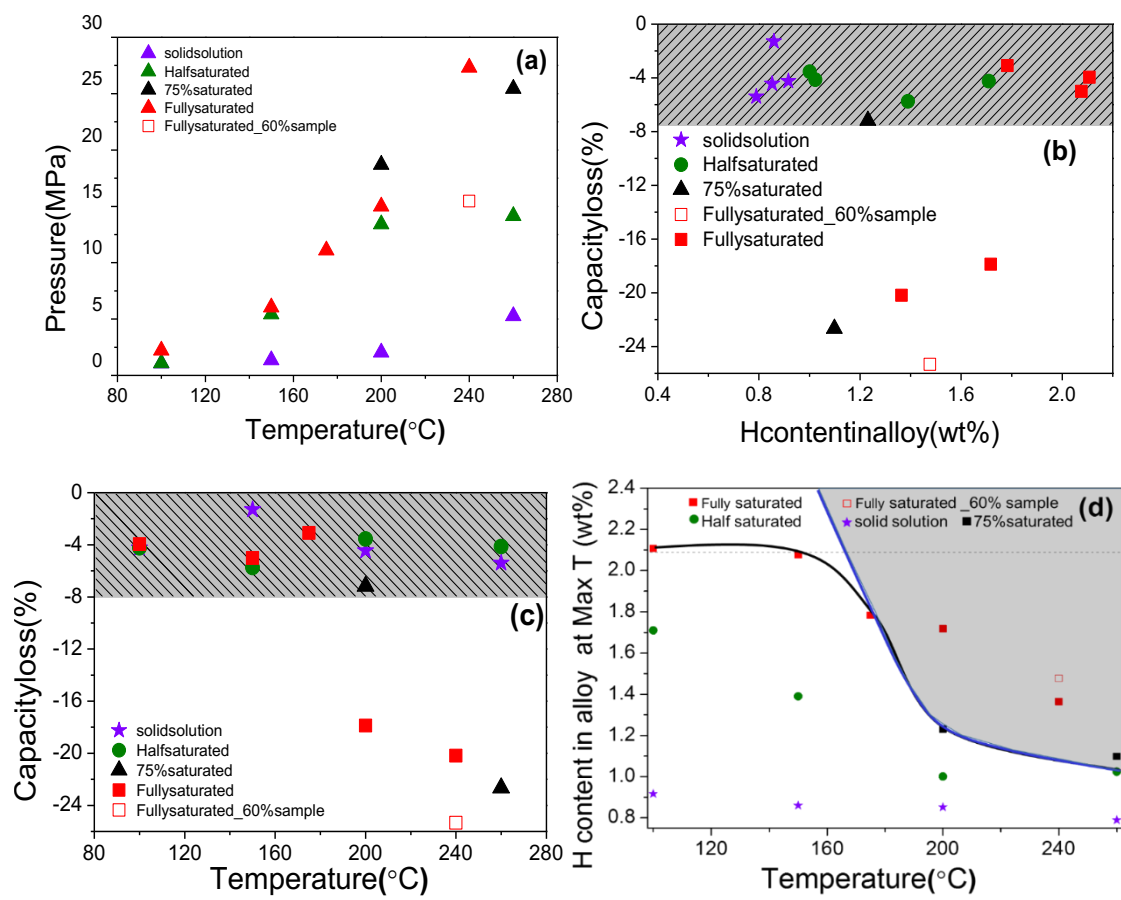


**Figure 4.19 (a) The achieved max pressure of sample cell at maximum temperature for each hydrogen compressor cycle measurement; (b) the capacity loss of each state with the changes of H content remained in the alloy at high temperature; (c) the capacity loss of each state with max temperature for hydrogen compressor cycle; (d) H content remained in the alloy at achieved max temperature.**

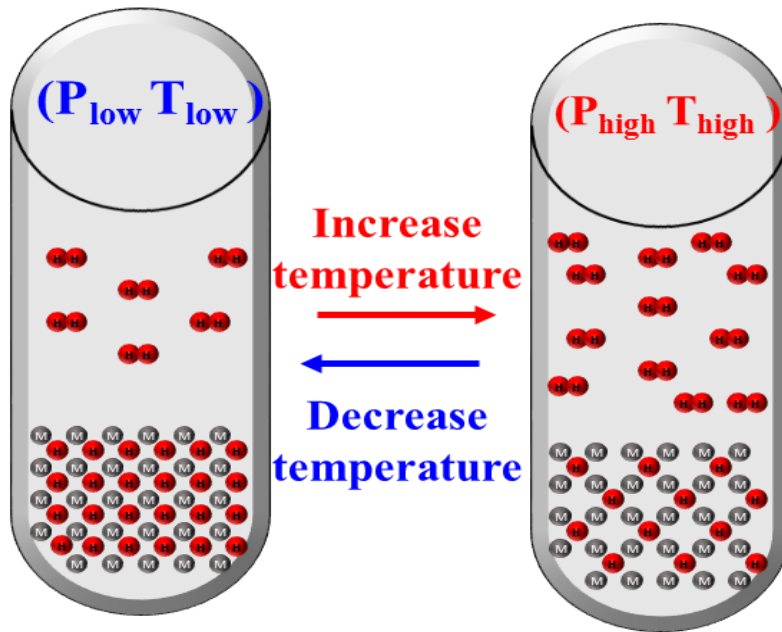


Figure 4.20 Illustration of pressure and temperature changes of hydrogen-metal system during thermal driven hydrogen compression process.

## Tables

Table 4.1. Atomic percentage of elements in  $V_{20}Ti_{32}Cr_{48}$  alloy as determined by EDS analysis. The point no. corresponds to the different positions as shown in Fig. 6 (b) and (d).

Point No.	V		Ti		Cr	
	Pristine	Cycled	Pristine	Cycled	Pristine	Cycled
1	19.42	10.54	32.84	63.81	47.74	25.65
2	20.02	11.63	32.01	59.39	47.97	28.98
3	19.40	9.29	32.61	67.69	47.99	23.01
4	19.14	16.23	33.00	44.98	47.86	38.80

Table. 4.2: Summary of detailed parameters for hydrogen compressor cycling test for  $V_{20}Ti_{32}Cr_{48}$  alloy at various conditions.

Percentage of filled $H_2$ /%	Initial Pressure/ MPa	Initial temperature / °C	Initial H content/ wt%	Aimed temperature / °C	Achieved max pressure/ MPa	Capacity losses/ %	H amount in the alloy /wt%
100	0.074	23.2	2.433	240	27.8	20.19	1.19
100	0.11	22	2.354	200	14.9	17.88	1.68
100	0.088	22.1	2.273	175	11	3.05	1.76
100	0.07	22	2.325	150	5.7	5.01	2.07
100	0.072	22.4	2.175	100	2.1	3.96	2.1
75	0.059	22.5	2.098	260	25.43	22.45	1.0
75	0.059	23.1	2.060	200	18.7	7.18	1.17
50	0.045	23	1.561	260	14.1	4.13	1.00
50	0.035	23.8	1.572	200	13.4	3.55	0.97
50	0.031	20.2	1.622	150	5.4	5.92	1.39
50	0.05	22.5	1.716	100	1.1	4.57	1.71
0	0.03	22.7	0.963	260	5.1	5.40	0.79
0	0.027	21	0.8329	200	7.8	4.45	0.85
0	0.021	22.2	0.876	150	1.3	1.30	0.86
0	0.03	22	0.917	100	1	4.24	0.92

## 5. Conclusions

In this thesis, in order to find the critical temperature and pressure conditions of degradation during thermochemical hydrogen compression of the  $V_{20}Ti_{32}Cr_{48}$  alloy, 25 hydrogen compressor cycles were performed by changing the hydrogen content and operation temperature using our homemade hydrogen compressor system. The hydrogen storage performance was evaluated by several experimental techniques. The main results obtained in this thesis are summarized as follows:

First of all, the hydrogen content influence on the cyclic durability of  $V_{20}Ti_{32}Cr_{48}$  alloy was investigated by checking the hydrogen storage capacity, the achieved maximum hydrogen compression pressure, structural and morphological properties. It was shown that hydrogen amount in the alloys plays an important role in the disproportion and degradation process during thermal-driven hydrogen compressor cycles. The hydrogen storage properties suggested that  $V_{20}Ti_{32}Cr_{48}$  alloy saturated with 75%  $H_2$  was deteriorated a lot after 25 hydrogen compressor cycles only at higher temperature, with hydrogen storage capacity reduction by more than 20% and sloppy plateau region. The increased slope indicated the possibility of multiple phases present in the sample, which dramatically reduced hydrogen compression efficiency. However, in the lower hydrogen

content cases,  $V_{20}Ti_{32}Cr_{48}$  alloy saturated with 50%  $H_2$  and solid solution, the hydrogen storage capacity losses were found negligible, *i.e.* 5.0 and 4.0% respectively, with similar slope in PCI curves, indicating the intact original hydrogen compression efficiency. The direct evidence was given by structure and morphology changes that were measured by XRD and SEM-EDS. It was concluded that the disproportionation occurred in the sample of  $V_{20}Ti_{32}Cr_{48}$  alloy with fully saturated  $H_2$ , were due to the appearance of  $VH_{0.88}$  and  $TiH_{0.66}$  phases. Interestingly, the sample saturated with 75%  $H_2$  and cycled up to 260 °C also showed a capacity decay, but no big changes in XRD peaks position were observed except the altered peak width and intensity that might be caused by stress/strains. Therefore, a conclusion was made that the disproportionation occurred by thermodynamically favored reactions was not the only reason for capacity fading, but the stress/strain generated in the material with higher amount of  $H_2$  during the compressor test may also be responsible for this degradation. As a key result, lower hydrogen content was found to be better for hydrogen compressor cyclic durability for  $V_{20}Ti_{32}Cr_{48}$  alloy whereas the large amount of stored hydrogen in alloy led to the reduction of reversible hydrogen storage capacity during hydrogen compression process for practical usage. This led to the reduction of compression efficiency and increase the maintenance cost.

Secondly, according to the investigation of temperature influence on the cyclic

durability of  $V_{20}Ti_{32}Cr_{48}$  alloy, lower temperature less than 200 °C was proved to be safe for hydrogen compression. The PCI curves of  $V_{20}Ti_{32}Cr_{48}$  alloy, fully saturated with  $H_2$  and cycled for hydrogen compressor up to 240 and 200 °C, showed significant hydrogen storage capacity loss up to 20.2 and 17.9%, respectively, which revealed the disproportion and degradation of the material. On the other hand, the fully saturated  $V_{20}Ti_{32}Cr_{48}$  alloy with  $H_2$  cycled up to 175, 150, and 100 °C and the  $V_{20}Ti_{32}Cr_{48}$  alloy with half saturated and solid solution showed little hydrogen capacity losses *i.e.* 4 to 5% with similar PCI slope.

The appearance of the new phases,  $VH_{0.88}$  and  $TiH_{0.66}$  in XRD pattern, and the Ti-rich phase found by SEM-EDS results clearly showed the disproportionation of  $V_{20}Ti_{32}Cr_{48}$  alloy with fully saturated  $H_2$ , cycled up to 240 °C that must be caused by thermodynamically favored reactions. The temperature of 200 °C may not be high enough to lead such kind of reactions but could be enough high to generate some lattice stress / strains in the alloy which caused the reduction in hydrogen storage capacity after compressor cycling test. Thus, lower temperature was found better for the compressor cyclic durability of  $V_{20}Ti_{32}Cr_{48}$  alloy whereas, higher temperature led the degradation of this alloy and reduced the hydrogen storage capacity during practical usage.

Based on the experimental facts obtained in this thesis, the boundary conditions of

hydrogen compressor cycle test for  $V_{20}Ti_{32}Cr_{48}$  alloy without disproportionation were defined as follows: the hydrogen content and temperature threshold of a model system *i.e.*  $V_{20}Ti_{32}Cr_{48}$  alloy for hydrogen compressor without disproportionation were identified as 75% and 200 °C, respectively. Hydrogen content as well as temperature both play important role in the disproportionation processes. According to the analysis of the cyclic durability of  $V_{20}Ti_{32}Cr_{48}$  alloy under various conditions, a clear disproportionation area was drawn for the first time which can be used as a guidance for the safe usage of  $V_{20}Ti_{32}Cr_{48}$  alloy for hydrogen compressor applications. This methodology can be applied to the other materials to identify the critical conditions required for their safer and stable operation during compressor cycling.

## References:

- [1] Züttel A. Hydrogen storage methods. Springer-Verlag (2004); 91,157–172.
- [2] Züttel A, Remhof A, Borgschulte A F. Hydrogen: the future energy carrier. Phil. Trans. R. Soc. A (2010); 368, 3329–3342.
- [3] Schlapbach L, Züttel A. Hydrogen-storage materials for mobile applications. Nature (2001); 414,353-358.
- [4] <https://www.japan.go.jp/g20japan/index.html>
- [5] Züttel A. Materials for hydrogen storage. Materials today (2003); 6-9, 24-33.
- [6] Lototsky M V, Yartys V A, Pollet B G, Bowman R C. Metal hydride hydrogen compressors: A review. Int. J. Hydrogen Energy (2014); 39, 5818-5851.
- [7] Bogdanović B. Magnesium hydride: A homogeneous-catalysed synthesis and its use in hydrogen storage. Int. J. Hydrogen Energy (1984); 9, 937-941.
- [8] Bogdanović B. Catalytic Synthesis of Organolithium and Organomagnesium Compounds and of Lithium and Magnesium Hydrides-Applications in Organic Synthesis and Hydrogen Storage. Angew, Chem. Int. Ed. Engl (1985); 24, 262-273.
- [9] Bogdanović B, Europ. Pat (1979); 3564.
- [10] B. Bogdanović, S. Liao, M. Schwickardi, P. Sikorsky, B. Spliethoff.

- Katalytische Synthese von Magnesiumhydrid unter milden Bedingungen. *Angew. Chem*(1980); 92, 845-846.
- [11] Niaz S, Manzoor T, Pandith A H. Hydrogen storage: Materials, methods and perspectives. *Renewable and Sustainable Energy Reviews* (2015); 50, 457–469.
- [12] Andrievski RA, Tarasov BP, Korobov II, Mozhina NG, Shilkin SP. Hydrogen absorption and electrocatalytic properties of ultrafine  $\text{LaNi}_5$  powders. *Int J Hydrogen Energy* (1996); 21, 11-12, 949-54.
- [13] Tarasov BP, Lototskii MV, Yartys VA. Problem of hydrogen storage and prospective uses of hydrides for hydrogen accumulation. *Russ J Gen Chem* (2007); 77, 4, 694-711.
- [14] Boser O. Hydrogen sorption in  $\text{LaNi}_5$ , *J Less Common Met* (1976); 46, 91-99.
- [15] Mordkovic V Z, Korostyshevsky N N, Baychtok Y K, Mazus E I, Dudakova N V, Mordovin V P. Degradation of  $\text{LaNi}_5$  by thermobaric cycling in hydrogen and hydrogen-nitrogen mixture. *Int J Hydrogen Energy* (1990); 1510, 723-726.
- [16] Kodama T. The thermodynamic parameters for the  $\text{LaNi}_{5-x}\text{Al}_x\text{-H}$  and  $\text{MmNi}_{5-x}\text{Al}_x\text{-H}$  systems. *J Alloys Compds* (1999); 289, 207-12.
- [17] Corre' S, Bououdina M, Fruchart D, Adachi G. Stabilisation of high dissociation pressure hydrides of formula  $\text{La}_{1-x}\text{Ce}_x\text{Ni}_5$  ( $x = 0-0.3$ ) with carbon monoxide. *J*

- Alloys Compds (1998); 275-277: 99-104.
- [18] Goodell PD. Stability of rechargeable hydriding alloys during extended cycling. J Less Common Met (1984); 99, 1-14.
- [19] Park J M, Lee J Y. The intrinsic degradation phenomena of LaNi<sub>5</sub> and LaNi<sub>4.7</sub>Al<sub>0.3</sub> by temperature induced hydrogen absorption-desorption cycling. Mat Res Bull (1987); 22, 455-65.
- [20] Shen CC, Perng TP. On the cyclic hydrogenation stability of an Lm(NiAl)<sub>5</sub>-based alloy with different hydrogen loadings. J Alloys Compds (2005); 392, 187-91.
- [21] Cheng HH, Yang HG, Li SL, Deng XX, Chen DM, Yang K. Effect of hydrogen absorption/desorption cycling on hydrogen storage performance of LaNi<sub>4.25</sub>Al<sub>0.75</sub>. J Alloys Compd (2008); 453, 448-52.
- [22] Baichtok Y K, Mordkovich V Z, Dudakova N V, Avetisov A K, Kasimtsev A V, Mordovin V P. Technological possibilities and state of the art in the development of hydride thermal sorption hydrogen compressors. Int Sci J Altern Energy Ecol (2004); 2, 10, 50-54.
- [23] Bowman Jr RC, Lindensmith CA, Luo S, Flanagan TB, Vogt T. Degradation behavior of LaNi<sub>5-x</sub>Sn<sub>x</sub>H<sub>z</sub> (x=0.20-0.25) at elevated temperatures. J Alloys Compd (2003); 330-2, 271-5.

- [24] Bowman Jr RC, Payzant EA, Wilson PR, Pearson DP, Ledovskikh A, Danilov D, et al. Characterization and analyses of degradation and recovery of  $\text{LaNi}_{4.78}\text{Sn}_{0.22}$  hydrides following thermal aging. *J Alloys Compd* (2013); 580, S207-10.
- [25] Mordkovich V Z, Korostyshevsky N N, Baichtock YuK, Dudakova NV, Mordovin V P, Sosna M H.  $\text{LaNi}_5$  and  $\text{Ce}_x\text{La}_{1-x}\text{Ni}_5$  changes in the course of thermobaric cycling in hydrogen and nitrogen/hydrogen mixture. *Int J Hydrogen Energy* (1993); 18(9), 747-9.
- [26] Friedlmeier G, Manthey A, Wanner M, Groll M. Cyclic stability of various application-relevant metal hydrides. *J Alloys Compd* (1995); 231, 880-7.
- [27] Wanner M, Friedlmeier G, Hoffmann G, Groll M. Thermodynamic and structural changes of various intermetallic compounds during extended cycling in closed systems. *J Alloys Compd* (1997); 253-254, 692-7.
- [28] Mungole M N, Balasubramaniam R. Effect of hydrogen cycling on the hydrogen storage properties of  $\text{MmNi}_{4.2}\text{Al}_{0.8}$ . *Int J Hydrogen Energy* (2000); 25, 55-60.
- [29] Nakamura Y, Oguro K, Uehara I, Akiba E. X-ray diffraction peak broadening and degradation in  $\text{LaNi}_5$ -based alloys. *Int J Hydrogen Energy* (2000); 25, 531-7.
- [30] Joubert J-M, Latroche M, Cerny R, Percheron-Guegan A, Yvon K. Hydrogen cycling induced degradation in  $\text{LaNi}_5$ -type materials. *J Alloys Compd* (2002);

- 330-332, 208-14.
- [31] Shen CC, Lee SM, Tang JC, Perng TP. Cyclic hydrogenation of an  $\text{LnNi}_5$ -based alloy with different hydrogen loadings. *J Alloys Compd* (2003); 356-7, 800-3.
- [32] Cheng H H, Yang H G, Li S L, Deng X X, Chen D M, Yang K. Effect of hydrogen absorption/desorption cycling on hydrogen storage performance of  $\text{LaNi}_{4.25}\text{Al}_{0.75}$ . *J Alloys Compd* (2008); 453, 448-52.
- [33] Li S L, Chen W, Chen D M, Yang K. Effect of long-term hydrogen absorption/desorption cycling on hydrogen storage properties of  $\text{MmNi}_{3.55}\text{Co}_{0.75}\text{Mn}_{0.4}\text{Al}_{0.3}$ . *J Alloys Compd* (2009); 474, 164-8.
- [34] Li S L, Chen W, Luo G, Han X B, Chen DM, Yang K, et al. Effect of hydrogen absorption/desorption cycling on hydrogen storage properties of a  $\text{LaNi}_{3.8}\text{Al}_{1.0}\text{Mn}_{0.2}$  alloy. *Int J Hydrogen Energy* (2012); 37, 3268-75.
- [35] Liu J, Li K, Cheng H, Yan K, Wang Y, Liu Y, et al. New insights into the hydrogen storage performance degradation and Al functioning mechanism of  $\text{LaNi}_{5-x}\text{Al}_x$  alloys. *Int J Hydrogen Energy* (2017); 42, 24904-14.
- [36] Obregón S A, Esquivel M R. Scheme of thermal compression of hydrogen (TCH) using  $\text{MmNi}_{4.25}\text{Al}_{0.75}$  recovered with ethyl alcohol and handled under non protective atmospheres. *Int J Hydrogen Energy* (2014); 39, 8577-8581.

- [37] Mainul M, Bhuiya H, Lee C Y, Hopkins R, Yoon H, Kim S, Park S H, Kim K J. A High-Performance Dual-Stage Hydrogen Compressor System Using  $\text{Ca}_{0.2}\text{Mm}_{0.8}\text{Ni}_5$  Metal Hydride. The American Society of Mechanical Engineers. Proceedings of the ASME 2011 Conference on Smart Materials, Adaptive Structures and Intelligent Systems. ASME 2011 Conference on Smart Materials, Adaptive Structures and Intelligent Systems, Volume 1. Scottsdale, Arizona, USA. September 18–21, 2011, 745-751.
- [38] Sekhar B S, Muthukumar P. Development of Double-Stage Metal Hydride–Based Hydrogen Compressor for Heat Transformer Application. *J ENERG ENG* (2015); 141, 4.
- [39] Li H, Wang X, Dong Z, Xu L, Chen C. A study on 70MPa metal hydride hydrogen compressor. *J Alloys Compd* (2010); 502, 503–507.
- [40] Boris P. Tarasov, Mikhail S. Bocharnikov, Yurii B. Yanenko, Pavel V. Fursikov B, Lototsky M V. Cycling stability of  $\text{RNi}_5$  (R = La, La+Ce) hydrides compressor. *Int J Hydrogen Energy* (2018); 43, 4415-4427.
- [41] Shilov A L, Padurets L N, Kost M E. Thermodynamics of hydrides of intermetallic compounds of transition metals. *Russ J Phys Chem* (1985); 59(8), 1857-75.

- [42] Sandrock G. A panoramic overview of hydrogen storage alloys from a gas reaction point of view, *J Alloys Compd* (1999); 293–295, 20, 877-888.
- [43] Tsurui N, Goshome K, Hino S, Endo N, Maeda T, Miyaoka H, Ichikawa T. Hydrogen Desorption Isobar Properties of  $Ti_{1.1}CrMn$  at High Temperatures and Pressures. *Materials Transactions* (2018); 59, 5, 855-857.
- [44] Reilly J J, Wiswall R H. Formation and Properties of Iron Titanium Hydride. *Inorganic Chemistry* (1974), 13, 1.
- [45] Zuchner H, Kirch G. Auger electron spectroscopy investigation of the activation of TiFe for hydrogen uptake. *Journal of the Less-Common Metals* (1984); 99, 143-150.
- [46] Blasius A, Gonser U. Mössbauer Surface Studies on TiFe Hydrogen Storage Material. *Appl. Phys* (1980); 22, 331-332.
- [47] Trudeau M L, Dignard-Bailey L, Schulz R. The oxidation of nanocrystal FeTi hydrogen storage compounds. *Nanostruct Mater* (1992); 1, 457-464.
- [48] Patel A K, Sharma P, Huot J. Effect of annealing on microstructure and hydrogenation properties of  $TiFe + X \text{ wt}\% \text{ Zr}$  ( $X = 4, 8$ ). *Int J Hydrogen Energy* (2018); 43, 12, 6238-6243.
- [49] Lv P, Huot J. Hydrogen storage properties of  $Ti_{0.95}FeZr_{0.05}$ ,  $TiFe_{0.95}Zr_{0.05}$  and

- TiFeZr<sub>0.05</sub>alloys. *Int J Hydrogen Energy* (2016); 41, 47, 22128-22133.
- [50] Chung H S, Lee J Y. Hydriding and dehydriding reaction rate of FeTi intermetallic compound. *Int J Hydrogen Energy* (1985); 10, 537–542.
- [51] Bratanich T I, Solonin S M, Skorokhod V V. Mechanical activation of hydrogen sorption with intermetallic compounds LaNi<sub>5</sub> and TiFe in powder systems. *Int J Hydrogen Energy* (1995); 20, 353–355.
- [52] Kulshreshtha S K, Jayakumar O D, Bhatt K B. Hydriding characteristics of palladium and platinum alloyed FeTi, *J Mater Sci* (1993); 28, 4229–4233.
- [53] Szajek A, Jurczyk M, Jankowska E. The electronic and electrochemical properties of the TiFe-based alloys, *J. Alloys Compd* (2003); 348, 285–292.
- [54] Suda T, Ohkawa M, Sawada S, Watanabe S, Ohnuki S, Nagata S. Effect of surface modification by ion implantation on hydrogenation property of TiFe alloy, *Mater. Trans* (2002); 43, 2703–2705.
- [55] Edalati E, Matsuda J, Arita M, Daio T, Akiba E, Horita Z. Mechanism of activation of TiFe intermetallics for hydrogen storage by severe plastic deformation using high-pressure torsion, *Appl. Phys. Lett* (2013); 103, 143902.
- [56] Edalati E, Matsuda J, Iwaoka H, Toh S, Akiba E, Horita Z, High-pressure torsion of TiFe intermetallics for activation of hydrogen storage at room temperature

- with heterogeneous nanostructure, *Int. J. Hydrogen Energy* (2013); 38, 4622–4627.
- [57] Edalati K, Matsuda J, Yanagida A, Akiba E, Horita Z. Activation of TiFe for hydrogen storage by plastic deformation using groove rolling and high-pressure torsion: similarities and differences, *Int. J. Hydrogen Energy* (2014); 39, 15589–15594.
- [58] Trudeau M L, Dignard-Bailey L, Schulz R, Tessier P, Zaluski L, Ryan D H, Strom-Olsen J O. The oxidation of nanocrystalline FeTi hydrogen storage compounds, *Nanostruct. Mater* (1992); 1, 457–464.
- [59] Haraki T, Oishi K, Uchida H, Miyamoto Y, Abe M, Kokaji T, Uchida S, Properties of hydrogen absorption by nano-structured FeTi alloys, *Int J Mater Res* (2008); 99, 507–512.
- [60] Emami H, Edalati K, Matsuda J, Akiba E, Horita Z. Hydrogen storage performance of TiFe after processing by ball milling. *Acta Materialia* (2015); 88, 190–195.
- [61] Kumar S, Jain A, Ichikawa T, Kojima Y, Dey GK. Development of vanadium based hydrogen storage material: A review. *Renew Sustain Energy Rev* (2017); 72, 791–800.

- [62] Veleckis E, Edwards RK. Thermodynamic Properties in the Systems V-H, Nb-H, and Ta-H Thermodynamic Properties in the Systems Vanadium-Hydrogen, Niobium-Hydrogen, and Tantalum-Hydrogen. *J Phys Chem C* (1969); 73, 3, 683-692.
- [63] Lototsky MV, Yartys VA, Zavaliy IY. Vanadium-based BCC alloys: phase-structural characteristics and hydrogen sorption properties. *J Alloys Compd* (2005); 404–406, 421–6.
- [64] Yukawa H, Takagi M, Teshima A, Morinaga M. Alloying effects on the stability of vanadium hydrides. *J Alloys Compd* (2002); 330–332, 105–9.
- [65] Yukawa H, Yamashita D, Ito S, Morinaga M, Yamaguchi S. Compositional dependence of hydriding properties of vanadium alloys at low hydrogen pressures. *J Alloys Compd* (2003); 356–357, 45–9.
- [66] Kumar S, Taxak M, Krishnamurthy N. Hydrogen absorption kinetics of V<sub>4</sub>Cr<sub>4</sub>Ti alloy prepared by aluminothermy. *Int J Hydrogen Energy* (2012); 37, 3283–91.
- [67] Peterson D T, Nelson S O. Isopiestic Solubility of Hydrogen in Vanadium Alloys at Low Temperatures. *Metall Mater Trans A* (1985); 16, 367–374.
- [68] Kumar S, Krishnamurthy N. Effect of aluminum on solubility and  $\beta$  phase stability of vanadium-hydrogen system. *Int J Refract Met Hard Mater* (2012); 35,

- 191–5.
- [69] Kumar S, Tiwari GP, Krishnamurthy N. Tailoring the hydrogen desorption thermodynamics of  $V_2H$  by alloying additives. *J Alloy Comps* (2015); 645, S252–S256.
- [70] Itoh H, Arashima H, Kubo K, Kabutomori T, Ohnishi K. Improvement of cyclic durability of BCC structured TiCrV alloys. *J Alloys Compd* (2005); 404-406, 417-20.
- [71] Shen C-C, Li H-C. Cyclic hydrogenation stability of  $\beta$ -hydrides for  $Ti_{25}V_{35}Cr_{40}$  alloys doped with carbon. *J Alloys Compd* (2015); 648, 534-9.
- [72] Selvaraj S, Jain A, Kumar S, Zhang T, Isobe S, Miyaoka H, et al. Study of cyclic performance of V-Ti-Cr alloys employed for hydrogen compressor. *Int J Hydrogen Energy* (2018); 43, 2881–2889.
- [73] Tarasov B P, Bocharnikov M S, Yanenko Y B, Fursikov P V, Lototskyy M V. Cycling stability of  $RNi_5$  ( $R= La, La+Ce$ ) hydrides during the operation of metal hydride hydrogen compressor. *Int J Hydrogen Energy* (2018); 43, 4415-4427.
- [74] H. H. van Mal. A  $LaNi_5$ -Hydride Thermal Absorption Compressor for a Hydrogen Refrigerator. *Chemie Ingenieur Technik*. (1973); 45, 2, 80-83.

- [75] E. P. Da Silva. Industrial prototype of a hydrogen compressor based on metallic hydride technology. *Int J Hydrogen Energy* (2018); 18, 4, 307-311.
- [76] Shmal'ko Y F, Ivanovsky A I, Lototsky M K, Volosnikov D V. Industrial Metal-Hydride Continuously-Operated Compressor. *Hydrogen Power: Theoretical and Engineering Solutions*, 323-32.
- [77] <http://ergenics.com/compression.html>.
- [78] Laurencelle F, Dehouche Z, Morin F, Goyette J. Experimental study on a metal hydride based hydrogen compressor. *J Alloys Compd* (2009); 475, 1–2, 810-816.
- [79] Cieslik J, Kula P, Filipek S M. Research on compressor utilizing hydrogen storage materials for application in heat treatment facilities. *J Alloys Compd* (2009); 480, 2, 612-616.
- [80] Popeneciu G, Almasan V, Coldea I, Lupu D, Misan I, Ardelean O. Investigation on a three-stage hydrogen thermal compressor based on metal hydrides. *Journal of Physics: Conference Series*, Volume 182, PROCESSES IN ISOTOPES AND MOLECULES 24–26 September, 2009, Cluj-Napoca, Romania.
- [81] Muthukumar P, Maiya M P, Murthy S S. Experiments on a metal hydride based hydrogen compressor. *Int J Hydrogen Energy* (2005); 30, 8, 879-892.

- [82] Selvaraj S, Jain A, Miyaoka H, Kojima Y, Ichikawa T. Hydrogen Sorption and Cyclic Compressor Performance of  $V_{40}Ti_{21.5}Cr_{33.5}M_5$  (M= Nb, Zr, Fe) Alloys. Journal of the Japan Institute of Energy (2019), 98, 157-164.
- [83] Sherif S A, Goswami D Y, Stefanakos E K, Steinfeld A. Handbook of Hydrogen Energy.
- [84] <https://webbook.nist.gov/chemistry/fluid/>